NETL

NATIONAL ENERGY TECHNOLOGY LABORATORY

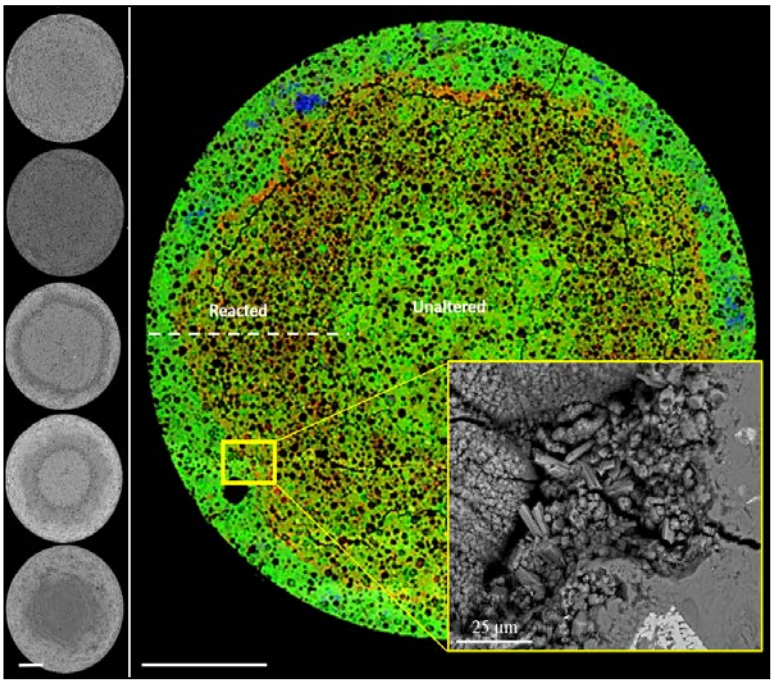

Foamed Cement Interactions with CO_2

23 January 2017

U.S. DEPARTMENT OF ENERGY | NATIONAL ENERGY TECHNOLOGY LABORATORY

Office of Fossil Energy

NETL-TRS-2-2017

Disclaimer

Cover Illustration: Qualitative SEM phase distribution map of the 30% foam quality cement sample after 56 days exposed to supercritical CO_2 environment. Colors are represented by blue = NaCl; orange= Mg,$CaCO_3$; and green= Ca-phases. Scale bar is 5 mm.

Suggested Citation: Verba, C.; Montross, S.; Spaulding, R.; Dalton, L.; Crandall, D.; Moore, J.; Glosser, D.; Huerta, N.; Kutchko, B. *Foamed Cement Interactions with CO_2*; NETL-TRS-2-2017; NETL Technical Report Series; U.S. Department of Energy, National Energy Technology Laboratory: Albany, OR, 2017; p 40.

An electronic version of this report can be found at:

http://netl.doe.gov/research/on-site-research/publications/featured-technical-reports

https://edx.netl.doe.gov/carbonstorage

Foamed Cement Interactions with CO_2

Circe Verba[1], Scott Montross[1,2], Richard Spaulding[3], Laura Dalton[2,5], Dustin Crandall[4], Jonathan Moore[5], Deborah Glosser[3], Nicolas Huerta[1], Barbara Kutchko[3]

[1] U.S. Department of Energy, National Energy Technology Laboratory, 1450 Queen Avenue SW, Albany, OR 97321

[2] Oak Ridge Institute for Science and Education (ORISE), U.S. Department of Energy, National Energy Technology Laboratory, 1450 Queen Avenue SW, Albany, OR 97321

[3] U.S. Department of Energy, Office of Research and Development, National Energy Technology Laboratory, 626 Cochrans Mill Road, Pittsburgh, PA 15236

[4] U.S. Department of Energy, National Energy Technology Laboratory, 3610 Collins Ferry Road Morgantown, WV 26507

[5] U.S. Department of Energy, National Energy Technology Laboratory, AECOM, 3610 Collins Ferry Road Morgantown, WV 26507

NETL-TRS-2-2017

23 January 2017

NETL Contacts:

Barbara Kutchko, Principal Investigator

Angela Goodman, Technical Portfolio Lead

Cynthia Powell, Executive Director, Research & Innovation Center

This page intentionally left blank.

Table of Contents

List of Figures

List of Tables

Acronyms, Abbreviations, and Symbols

Term	Description
2D	Two-dimensional
3D	Three-dimensional
BSD	Bubble size distribution
BSE	Backscattered electron
C_2S	Dicalcium silicate
C_3S	Tricalcium silicate
CO_2	Carbon dioxide
CT	Computed tomography
EOR	Enhanced oil recovery
GCS	Geologic carbon storage
GoM	Gulf of Mexico
IPA	Isopropanol
NER	New England Research Group
PDP	Pulse decay permeability
SACROC	Scurry Area Canyon Reef Operators Committee
SC-CO_2	Supercritical CO_2
S.D.	Standard deviation
SEM	Scanning electron microscopy
w/c	Water to cement ratio

Acknowledgments

This work was completed as part of National Energy Technology Laboratory (NETL) research for the U.S. Department of Energy's (DOE) Carbon Storage Program. The author wishes to acknowledge Cindy Powell and Traci Rodosta (NETL Research and Innovation Center) as well as Angela Goodman (NETL Technical Portfolio Manager Carbon Storage) for guidance, direction, and support.

The authors wish to acknowledge Jeff Oberfoell for laboratory assistance as well as Dustin McIntyre and Bryan Tennant for computed tomography assistance.

EXECUTIVE SUMMARY

Geologic carbon storage (GCS) is a potentially viable strategy to reduce greenhouse emissions. Understanding the risks to engineered and geologic structures associated with GCS is an important first step towards developing practices for safe and effective storage. The widespread utilization of foamed cement in wells may mean that carbon dioxide (CO_2)/brine/foamed cement reactions may occur within these GCS sites. Characterizing the difference in alteration rates as well as the physical and mechanical impact of CO_2/brine/foamed cement is an important preliminary step to ensuring offshore and onshore GCS is a prudent anthropogenic CO_2 mitigation choice.

In a typical oil and gas well, cement is placed in the annulus between the steel casing and formation rock for both zonal isolation and casing support. The cement must have sufficient strength to secure the casing in the hole and withstand the stress of drilling, perforating, and fracturing (e.g. API, 1997, 2010 Worldwide Cementing Practices). As such, measuring the mechanical and properties of cement is an important step in predicting cement behavior under applied downhole stresses (Nelson, 2006). Zonal isolation is the prevention of fluids migrating to different zones outside of the casing and is strongly impacted by the permeability of the wellbore cement (Nelson, 2006). Zonal isolation depends on both the mechanical behavior and permeability (a physical property) of the cement (Mueller and Eid, 2006; Nelson, 2006). Long-term integrity of cement depends on the mechanical properties of the cement sheath, such as Young's Modulus (Griffith et al., 2004). The cement sheath's ability to withstand the stresses from changes in pressure and temperature is predominantly determined by the mechanical properties, including Young's modulus, Poisson's ratio, and tensile strength. Any geochemical alteration may impact both the mechanical and physical properties of the cement, thus ultimately impacting the structural integrity of the wellbore.

In this study, atmospheric foamed cements were generated using a neat cement and three foam qualities (volume of entrained gas in the cement) - 10%, 20%, and 30 % gas volume. The samples were immersed in a 0.25 M NaCl brine followed by the injection of supercritical CO_2 at 28.9 MPa and 50°C. Petrophysical properties were examined for representative samples using computed tomography (CT) and scanning electron microscopy (SEM). CT scanning of representative samples across the range of reacted cements revealed macroscopic changes in structure due to brine/CO_2/cement interactions. The high foam quality samples resulted in more CO_2-saturated brine infiltrating radially deeper into the cement and thus were more susceptible to alteration. After 56 days of exposure, the 30% foam quality sample had the most reaction resulting in an alteration depth of 8.35 ± 0.13 mm with a calculated 34.6 ± 0.2% reacted area and 5.76 ± 0.2% reacted pore space area. The neat sample on the other hand, had a reaction depth of 0.31 ± 0.13 mm with a calculated 0.15 ± 0.08% reacted area and 0.57 ± 0.05% reacted pore area. Physical measurements of the exposed samples were consistent with this degree of alteration having 47.02% porosity and the highest permeability of 0.041 mD. These results indicate that the greater surface area provided by the increase of pore space in the higher quality foam coupled with carbonate diffusion reactions enabled greater alteration.

1. INTRODUCTION

Offshore formations in the Gulf of Mexico (GoM) are currently being evaluated for geologic carbon storage (GSC) in the United States. The goal of this work is to evaluate the impact of injecting carbon dioxide (CO_2) into existing wells that were constructed using foamed cement and characterize the interaction between foamed cement/CO_2/brine that may be encountered during large scale GCS operations in both offshore and onshore wells. This research is also applicable for onshore CO_2 injection for enhanced hydraulic fracturing or to mitigate gas migration issues. Foamed cement is the preferred material to case zones that are weak and incapable of supporting the weight of regular cement as outlined in American Petroleum Institute (API) RP 65 (API, 2010). Offshore wells that pass through zones of sand, with fairly high permeability and porosity are potential targets for GCS injections and therefore it is important to understand how existing foamed cement and injected CO_2 will interact.

Carbon storage is a viable strategy for reducing CO_2 emissions; however, numerous studies have shown that in simulated downhole conditions CO_2 interactions with the wellbore system—including cement, host rock and/or casings—result in alteration and potential degradation of the cement that can adversely affect wellbore integrity (e.g. Kutchko et al., 2008; Barlet-Gouédard, 2012; Huerta et al., 2013). To mitigate shallow hazards in deepwater Gulf of Mexico, foamed cement systems are recommended by API for zonal isolation and preventing compaction damage in deepwater operations (API-65 2010). Isolation of preferential flow paths is accomplished by pumping cement down the borehole and up into the annulus following API 65 Standard (API Standard 65-Part 2, 2010). Properties of foamed cement and use in cementing of fragile-formation wells is reviewed by Harms and Febus (1985). Kutchko et al. (2014) provided the first assessment of the properties and structure of foamed cement used in deep offshore wells.

The primary function of cement in wells is to provide support for the casing string and zonal isolation for the life of the well (Iverson et al., 2008). Zonal isolation depends on the physical and mechanical attributes of the cement. It is necessary that the cement used is capable of supporting the casing as well as preventing the migrations of subsurface fluids into and out of the wellbore environment. In addition, the cement must be durable to withstand attack by corrosive gas, brine, or in the cases of GCS the injection of acid gas (i.e. CO_2). Cement failure or poor bonding could be a source of gas migrating to the surface.

1.1 CARBON DIOXIDE STORAGE IN GEOLOGIC FORMATIONS

There is no single technology that will provide emissions reductions while meeting the energy demands of a growing population with increasing energy consumption (IPCC, 2007). However, carbon capture and storage (CCS) could potentially prevent the release of 25 Gt of carbon by the year 2050 if used in conjunction with power generation plants (Pacala and Socolow, 2004).

CCS is the process by which CO_2 is isolated from effluent waste streams at major point sources (power plants, oil processing facilities, and concrete production facilities) and injected underground to prevent its release to the atmosphere (White, 2003). Some of the potential targets for CCS are depleted oil and gas reservoirs, deep unmineable coal seams, and deep brine or saline aquifers (Thomas, 2005; White, 2003; Benson and Surles, 2006; Gibbins and Chalmers, 2008). Each target has distinct characteristics that are expected to influence the overall storage efficacy. The applicability of using deep water reservoirs in the GoM has been recognized.

Volume estimates for offshore the lower 48 states has the potential to sequester ~3,600 Gt of CO_2 with most of the storage potential in saline reservoirs in the GoM (Vidas et al., 2012).

CO_2 exists in the supercritical (SC-CO_2) phase when pressure and temperature conditions exceed a thermodynamic critical point at depths greater than 800 m and where conditions exceeding 31.2°C and 7.4 MPa exist. In the supercritical state, CO_2 is in a mixed gas/liquid phase where the viscosity is that of the gas phase and density similar to the liquid phase. The state and fluid dynamics of SC-CO_2 make it highly reactive (Sengers, 1994). Supercritical CO_2 can dissolve into fluids (e.g., brines or formation water) and is generally more reactive than the gas phase (Sengers, 1994). The characteristics of SC-CO_2 allow it to be injected into pressurized and fluid saturated formations and allows for maximum CO_2 mass per unit volume of rock porosity (Span and Wagner, 1996; Holloway, 1997).

Efficacy of CO_2 storage is impacted by: physical – porosity, permeability, pressure, temperature, fracture networks (Anderson and Newell, 2004); chemical – mineralogy, formation water chemistry, and gas chemistry; and the logistical – CO_2 source, pipelines, well infrastructure – constraints associated with GSC operations such as creation of leakage pathways and the accessibility of target formations (Gasda et al., 2013; Boukhelifa et al., 2004). The permeability and integrity of the cement in the annulus and in the well determine how effective the seal is for preventing leakage. However, maintaining wellbore integrity during CO_2 injection and storage is the biggest risk contributing to leakage of CO_2 from underground storage sites (Carey et al., 2007). The most likely route for leakage of CO_2 to the surface from subsurface storage is through the wellbore (Gasda et al., 2013). In a typical oil and gas well, cement is placed in the annulus between the steel casing and formation rock to prevent leakage or communication of fluids zones. Abandoned or decommissioned wells are additionally sealed with cement to block the vertical migration of fluids within the well itself. Leakage of injected CO_2 can occur through cracks, joints in the casing, or carbonated brine can infiltrate through the annular space and migrate unintended into porous non-confining rock formations. For a cement to be effective it must be able to maintain low permeability and resistance to dissolution over long term (>1,000 years) exposure to high CO_2 conditions at elevated temperature and pressure (Kutchko et al., 2008).

1.2 DEGRADATION OF CEMENT SYSTEMS IN THE PRESENCE OF CO_2

When Portland cement is mixed with water its compounds form hydration products (Table 1). The main hydration products formed are calcium silicate hydrate gel (C-S-H) and calcium hydroxide ($Ca(OH)_2$). C-S-H is a semi-amorphous, gel-like material that makes up nearly 70% of the cement and is the primary binding material. $Ca(OH)_2$ is the crystalline component and comprises 15–20 wt% of the hydrated cement (Nelson and Guillot, 2006). The mechanical properties of the cement are determined by many factors, including its mineralogical content (Table 1), degree of hydration, and density (Huerta et al., 2013). Cement systems exposed to CO_2 injection must maintain long-term structural integrity. Portland cement is commonly used in subterranean cementing applications.

Table 1: Composition of typical Class H Portland cement

Cement Compound	Weight Percent (%)	Chemical Formula
Tricalcium silicate	50	Ca_3SiO_5 or $_3CaO{\cdot}SiO_2$
Dicalcium silicate	25	Ca_2SiO_4 or $_2CaO{\cdot}SiO_2$
Tricalcium aluminate	10	$Ca_3Al_2O_6$ or $_3CaO{\cdot}Al_2O_3$
Tetracalcium aluminoferrite	10	$Ca_4Al_2FeO_{10}$ or $_4CaO{\cdot}Al_2O_3{\cdot}Fe_2O_3$
Gypsum	5	$CaSO_4{\cdot}H_2O$

Conventional Portland cement based systems are thermodynamically unstable in CO_2-rich environments and tend to degrade more rapidly when exposed to acid/sour gas (Randhol et al., 2007). Carbonic acid may be naturally present in a subterranean formation, or it may occur by the reaction of subterranean water and CO_2, when the latter has been introduced into the wellbore environment during GCS. The amount of CO_2 diffused into cement is related to the permeability and porosity of the cement. As CO_2 laden fluids diffuse into the cement matrix, and dissociation products, specifically carbonic acid (H_2CO_3), are free to react with calcium hydroxide and calcium silicate hydrate in the cured cement. The soluble reaction products (e.g., Ca^{2+}, $(OH\text{-})^2$, CO_3^{2-}, or HCO_3^-) migrate out of the cement matrix leading to a decrease in compressive strength and an increase in permeability (Thaulow et al., 2001). In addition, chloride and hydrogen sulfide ions, present in subsurface fluids, can penetrate the cement sheath and adversely affect or react with the steel casing (Kutchko et al., 2011). Degradation of the cement and casing increases the risk for interzonal communication of fluids and loss in zonal isolation.

Alteration of Portland cement and cement/steel casing by CO_2 have been studied extensively (Carey et al., 2007; Kutchko et al., 2008; Newell and Carey, 2013; Nasvi et al., 2014). Cement-CO_2 equilibrium is a complex set of reactions–as CO_2 dissolves into solution and subsequently diffuses into the cement paste, the pH of the cement is reduced from 12.4 to 6.3-10.3 (e.g. Thaulow et al., 2001). The reduction in alkalinity results in less protection against acid attack to the cement matrix or steel casing. In cases where a low-density foamed cement is in use, such as a well, carbonation may be turned into an advantage for strengthening and reducing the permeability of the cement system. Cement additives (e.g., pozzolan) offer some reduction in carbonation by the pozzolan reacting with the calcium hydroxide that is formed by the hydration of the cement (Kutchko et al., 2009). This reaction forms calcium aluminosilicates that offer some resistance to degradation by CO_2. Reinforcing materials, or sections of casing in proximity to cement where the pH is lower, are not as well protected from corrosion as materials in contact with cement that is at a higher pH. The penetration of CO_2 into the cement results in a change of pH creating a carbonation front. The proposed mechanism of alteration of Portland cement by CO_2 is shown in the following reactions:

$$CO_2 + H_2O \rightarrow H_2CO_3 \quad (1)$$

$$H_2CO_3 + C\text{-}S\text{-}H \rightarrow silica\ gel + CaCO_3 \quad (2)$$

$$H_2CO_3 + Ca(OH)_2 \rightarrow CaCO_3 + 2H_2O \quad (3)$$

$$H_2CO_3 + CaCO_3 \rightarrow Ca(HCO_3)_2 \quad (4)$$

Leakage due to chemical diffusion by SC-CO_2 through neat cement is not a significant concern as shown in previous studies (Kutchko et al., 2008). These studies used cured cement samples partially immersed in NaCl-brine inside a vessel pressurized with CO_2; the authors showed that curing conditions (e.g., high temperature and high pressure) resulted in a change in the microstructure. Cement cured at 50°C and 30.3 MPa, representing geologic storage conditions, was more resistant to carbonic acid attack than cement cured under atmospheric conditions (e.g., 22°C and 0.1 MPa). In these laboratory studies Kutchko et al. (2008) performed SEM analysis of cement exposed to CO_2 saturated brine under storage conditions. The study results revealed three distinct zones of alteration: 1) an outer porous zone; 2) an intermediate precipitation zone; and 3) an inner zone leached of calcium hydroxide. Alteration of the cement has been shown to occur through matrix diffusion or diffusion through preexisting gaps or fractures (Kutchko et al., 2008). Carbonation within the inner precipitation zone serves as a gap filling process that precipitates calcite within the pores and matrix leading to decrease in permeability and strength (Kutchko et al., 2008). Other studies agree with the conclusion that well cement alteration can occur under storage conditions. Scherer et al. (2011) analyzed cores retrieved from the Teapot Dome, a 19-year old well. Their results indicate that significant modification of the well cement occurred and that the cement of existing wells considered for CO_2 injection and storage should be scrutinized in order to address the implications of pre-injected alteration. Experimental data indicate that coupled flow and reaction pathways lead to conditions that favor precipitation-induced fracture sealing which possibly leads to a reduced leak rate over time (Huerta et al., 2016). Acid gas and co-storage experiments by Kutchko et al. (2011) show that H_2S is detrimental to cement, however less so when CO_2 is present.

1.3 FOAMED CEMENT SYSTEMS

Foamed cement is a “system” containing cement, foam stabilizer, gas, and water. Foamed cement is created when a gas, typically nitrogen, is stabilized as microscopic bubbles in the cement matrix (Harms and Febus, 1985; Nelson and Guillot, 2006). The entrained gas bubbles in the cement create a network of void spaces and give the cement more elasticity than conventional cement. The use of foamed cement in isolating problem geologic formations in the GoM is well documented in the literature (Kutchko et al., 2014; Benge and Poole, 2005; Harlan et al., 2001; White et al., 2000; Kopp et al., 2000; Frisch et al., 1999; Benge et al., 1996; Thayer et al., 1993; Harms and Febus, 1985). Major technological improvements in cement production, including development of more stable surfactants and foaming agents, and methods for cement delivery have led to the widespread use of foamed cement as the primary material for casing support and zonal isolation in deepwater wells (see Kutchko et al., 2014; Benge and Poole, 2005; Benge et al., 1996; Harlan et al., 2001; Rae and Lullo, 2004). Low-density foamed cement is more ductile than conventional cement and can tolerate expansion, shrinking, and displacement without losing its sealing capabilities (Spielman et al., 2006). In addition to its light-weight property, foamed cement has excellent resistance to temperature and fluid-induced stresses (e.g. Dusterhoft, 2003).

Foamed cement cured under laboratory controlled carbonation conditions has shown accelerated carbonation via the hydration of tricalcium silicate (C_3S) and dicalcium silicate (C_2S) when reacted with CO_2, potentially resulting in improved cement strength via the hydration of C_3S and C_2S (Chen et al., 2011). Sulaiman et al. (2011) investigated the permeability and carbonation of foamed concrete with varying foam qualities. In laboratory experiments the rate of carbonation was inversely proportional to the square root of the density of the cement system (Sulaiman et

al., 2011). It is unclear whether foamed cements would have a similar relationship between degradation and carbonation given the contrasting initial physical properties of cement versus concrete. Knowledge of carbonation rates of different foamed concrete qualities (gas volume) are limited. Jones and McCarthy (2005) showed that lower density concrete carbonates at a higher rate than traditional cement. Carbonation rates for foamed cement reported by Brady (2001) were reported to be 5.7 mm/year and at least 50% higher than reported by Bamforth (1998) for normal weight concrete having the same cement content. The carbonation resistance of relatively high strength, foamed concrete is much lower than that of normal weight concrete. Dhir and Jones (1999) discovered over an approximate 3-month period the depth of carbonation in a foamed cement/sand mix, having a density of 1,400 kg/m^3, was in excess of 20 mm. The much higher resistance of the denser foamed concrete was attributed to its structure and higher cement content.

1.4 BUBBLE SIZE DISTRIBUTIONS, MECHANICAL, AND PHYSICAL PROPERTIES OF FOAMED CEMENT

Foamed cement is generated at the surface of a well pad or rig and is then pumped into a well through high pressure treating lines. The process of generating and placing foamed cement in an annulus may affect the final properties and performance of the cement (Kutchko et. al., 2015). API RP 10B-4 is the current industry standard for ensuring the stability of the foamed cement before it is pumped down the well. The properties and stability of the foamed cement are believed to be greatly affected by temperature, pressure, and strain rate.

A stable, laboratory generated foamed cement should have a uniform distribution of spherical and discreet bubbles to ensure that gas will not break out of the slurry (Nelson, 2006; Griffith et al., 2004). An unstable foamed cement may contain non-spherical and/or interconnected voids, which can result in poorly contained sections, channeling in the well and density inconsistencies across the column (Nelson, 2006; de Rozieres and Ferriere, 1991). These foamed cements may have lower compressive strength and higher permeability than stable foamed cements (Nelson, 2006).

Analysis of laboratory generated foamed cement was preformed using CT imaging to visualize and conduct statistical analysis of bubble size distributions (BSD; Kutchko et al., 2013). CT images were used to calculate air volume (pores) values which were consistent with the indicated foam quality; Kutchko et al. (2013) and Gill et al. (2014) demonstrated the merit in using CT scanning and image analysis to assess the stability of foamed cement systems. Atmospherically-generated foamed cement were found to linearly decrease in compressive strength as the volume of entrained air increased and become more elastic (lower Young's modulus). Specifically, a 40% foamed cement decrease in compressive strength and Young's modulus by at least 60% as compared to the 10% foam quality sample (Kutchko et al., 2014).

The permeability of atmospheric-generated foamed cement appears to correlate with porosity, the BSD, and connectivity of the bubbles and matrix pore spaces (Spaulding, 2015). Several processes can occur during cement curing, including bubble coalescence and segregation. Coalescence or coarsening of bubbles in the cement matrix can lead to a reduction in stability of the cement. Bubbles might also migrate to the surface of the cement sheath before the cement hardens. This is one of the mechanisms that is tested for in the API RP10-b (API, 1997) and denotes the cement as unstable and unusable in the wellbore.

2. METHODS

2.1 CEMENT SLURRY-SAMPLE PREPARATION

The cement slurries were prepared using a Class H Portland cement provided by Lafarge with a base slurry density of 16.5 lbm/gal (1.97 g/cm^3) and a water to cement ratio (W/C) of 0.38. Foamed cement samples were prepared according to API RP 10B-4 using an Ametek (Chandler Engineering) constant speed mixer (model 30-60). Once the base slurry was mixed, it was poured into a stainless steel, screw-top blender with a stacked blade assembly to provide the proper amount of shear (Galiana et al., 1991). Atmospheric foamed cements contain predefined amounts of air, as a percentage of the total cement volume. One group of Class H neat cement, which does not have added entrained gas, was created to use as a control for comparison. Foamed cements of 10%, 20%, and 30% entrained air fractions were mixed using industry standard foaming agents (provided by industry collaborators). Once mixed, the slurries were poured into prepared 25.4-cm diameter cylindrical molds and allowed to cure for 3 days under atmospheric pressure at 50°C. The samples were removed after 3 days and placed into a water bath to continue curing for 25 more days (28 days total). After curing, the samples were removed from the bath, labeled, and weighed. Samples that were to be analyzed with CT and SEM were placed in plastic bottles and submerged in the same (deionized) water used for the initial curing. Samples for porosity/permeability measurements were put in a desiccator to dry. Subsequent measurements of weight were taken until the weights remained consistent over time (~14–21 days), thus ensuring the samples were sufficiently dry for gas permeability measurements (per methods of Mindess and Young, 1981). All samples were dried at atmospheric pressure and temperature to avoid damaging them by thermally stressing or over desiccating (Nelson and Guillot, 2006).

2.2 POROSITY, PERMEABILITY, AND VELOCITY MEASUREMENTS

2.2.1 Helium Porosimetry

Sample diameters and lengths were measured using an electronic caliper and the results recorded digitally. The samples were placed into a Helium porosimeter (HP 401, TEMCO, Inc.) and the Smartporosity computer program was used to determine porosity. The HP 401 is able to measure porosity levels as low as 1% with relative precision.

2.2.2 Permeability

Nitrogen permeability was measured using a constant flow permeameter: Temco UltraPerm 500 Permeameter with a Corelab WinPerm computer program. The permeability was estimated using Darcy's Law (Equation 1):

$$\boldsymbol{K = \frac{Qnl}{S\Delta p}} \quad (1)$$

Where *n* is the viscosity of nitrogen at atmospheric conditions (0.017631 cP), *l* is the sample length, and *S* is the cross-sectional area of the cement sample. Due to gas slippage, a Klinkenburg correction was applied for permeability measurements.

Pulse decay permeability (PDP) was also measured using a CoreLab PDP-200. This technique establishes a set pore pressure throughout a core, then sends a differential pressure pulse through the length of the sample. The computer program records the change in pressure across the sample, the pressure downstream, and the time it takes to travel the length of the core and uses these parameters to determine permeability.

2.2.3 Ultrasonic-Waveforms and Velocity Measurements

All velocity measurements were made using the New England Research Group (NER) AutoLab 1500 device. This device is capable of triaxial compression and temperature control, allowing the user to control the confining, pore, and effective pressures as well as the temperature exposed to the cement samples (specification are in the Appendix). In addition, the AutoLab 1500 also has two ultrasonic wave transducers, which generate ultrasonic P and S waves in one end of the core and records the arrival of the waves at the other end. The device also records sampling frequency, wave velocity, and physical characteristics like Young's modulus and Poisson's ratio. All samples were subjected to 1 cycle (ramped up and then down) of effective pressures ranging from 8.2 MPa to 40.2 MPa, with Young's modulus and Poisson's ratio measurements being taken every 4 MPa step.

Young's modulus and Poisson's ratio values were determined from shear and compressional wave velocities using Equations 2 and 3 where E = Young's Modulus, ρ = Bulk density, V_s = Shear wave velocity, V_p = Compression wave velocity, ν = Poisson's Ratio (Murayama et al., 2013).

$$E = \frac{\rho V_S^2 (3V_P^2 - 4V_S^2)}{V_P^2 - V_S^2} \quad (2)$$

$$\nu = \frac{1 - 2(V_S/V_P)^2}{2[1 - (V_S/V_P)^2]} \quad (3)$$

Additionally, shear modulus (μ), bulk modulus (K), and the first Lame′ parameter (λ) were calculated using the formulas (4–6) below for isotrophic material (De Beer and Maina, 2008).

$$\mu = \frac{E}{2+2\nu} \quad (4)$$

$$K = \frac{E}{3(1-2\nu)} \quad (5)$$

$$\lambda = \frac{E\nu}{(1+\nu)(1-2\nu)} \quad (6)$$

2.3 CEMENT SAMPLE EXPOSURE TO CO_2-BRINE

The cement samples were exposed using equipment in the High Pressure Immersion and Reactive Transport Laboratory at NETL's Albany site. The equipment used was a system consisting of four Parr standing stirred autoclaves. Four different cement formulations were used: Neat, 10%, 20%, and 30% foam quality. Five samples of each formulation were generated

for this study for a total of twenty samples. The samples were stored in 1 L of deionized water (from the curing step) before exposure. One sample of each formulation was placed within an autoclave, now referred to as reacted samples, and one sample was set aside as a control, an unreacted sample. The target exposure conditions for the experiment were pressure and temperature at 28.9 MPa and 50°C respectively. The experiment conditions for each autoclave are shown in Table 2. Briefly, the cement samples were submerged in a 0.25 M NaCl brine saturated with CO_2. At the end of each exposure time the samples were removed from the autoclave. The pH of the brine was measured immediately. An additional 50 mL of brine was collected for chemical analysis. The reacted cores were placed in a 1 L plastic bottle with the remaining brine and stored at room temperature until analysis.

Table 2: Autoclave conditions during exposure with the standard deviation (S.D.) of conditions

	Time		Temperature (°C)		Pressure (MPa)	
Autoclave ID	Exposure Duration (days)	Sample ID (days)	Average	S.D.	Average	S.D.
AC1	55.84	56	49.9	2.0	28.6	2.2
AC2	27.78	28	51.0	1.2	28.7	2.2
AC3	13.78	14	49.7	4.1	28.4	3.0
AC4	6.83	7	49.8	2.8	29.0	0.6

2.4 COMPUTED TOMOGRAPHY

All of the different foam quality samples that experienced 56 days of exposure to SC-CO_2/brine at the conditions described above were non-destructively imaged before and after reaction at NETL's CT scanning facility in Morgantown, West Virginia. A North Star Imaging M-5000 system was used to scan each 17.5 cm (3 in.) long sample in five sections. Scanning smaller sections of the core was performed to achieve the higher resolution of 15.2 μm/voxel. This resolution of the imaging does not have the fidelity to discern the porosity within the cement matrix, but did enable characterization of reacted zones, larger trapped bubbles (greater than ~10 μm), and features of interest within the cores.

Samples were scanned at an energy of 185 kV, 200 mA, and 1,440 radiographs were obtained prior to reconstructing the two-dimensional (2D) X-ray images into a three-dimensional (3D) volume using the North Star Imaging EFX-CT software. No beam hardening or imaging filters were used. All post processing was performed with programs ImageJ (Rasband, 2016) and Ilastik (Sommer et al., 2011). After scanning samples were sent to NETL Pittsburgh for further analysis.

2.5 SCANNING ELECTRON MICROSCOPY AND X-RAY MICROANALYSIS

2.5.1 Sample Preparation

The unreacted and reacted cement cores were dried in a desiccator purged with nitrogen. Two 1-cm thick slices were cut from the bottom of each of the unreacted and reacted cores (see Figure 1) using a tile saw lubricated with 99% pure isopropanol (IPA). Material leftover from cutting was removed from the sample by rinsing and soaking the sample with IPA. Cleaned samples were dried in a N_2 desiccator and stored under N_2 atmosphere. Dried samples were photographed using a Nikon, cut for XRD (bottommost piece) and prepared for electron microscopy. The 1 in. diameter samples were mounted in 1.25 in. holders with cold-press epoxy 5:1 (epoxy to hardener). The bottom of the holder was filled with enough epoxy (~2 mL) to hold the cement sample in the center of the base of the mount. The remaining epoxy (~10 mL) was poured slowly and in a circular fashion around the edges of the cement sample to minimize turbidity during delivery of the epoxy and keep the sample from floating off the base of the mount. The epoxy mount was degassed in a vacuum chamber. The epoxy cured overnight at ambient laboratory conditions and then was placed in the nitrogen atmosphere desiccator until fully cured (~24 hrs).

The mounted sample was manually ground in sequential steps using a Secotom Grinder Polisher with 80, 220, 400, 500, 600, 1,200-grit diamond discs. IPA was used as a lubricant during all grinding/polishing steps, to clean the grinding discs between samples, and to remove grinding waste from the sample. After grinding, the samples were pre-polished in three steps using 6-micron, 4-micron, and 1-micron silica polishing beads in IPA. A 0.05-micron Al polish was used for the final polish. The polished samples were soaked in IPA for 10 min then lapped with an IPA saturated Chem-Met polishing pad. All samples were stored in a nitrogen atmosphere desiccator until needed.

2.5.2 SEM and Microanalysis

Polished samples were electro-coated with a ~10 nm of Pt prior to SEM analysis. Backscattered electron (BSE) images were collected using a FEI Inspect V field emission electron microscope equipped with an Oxford INCA X-ray detector. All imaging and X-ray analysis were done at 15 keV. Backscattered electron images and X-ray spectra were collected for each sample (up to 4088 fields of view per 1-in. diameter core) and montaged using the INCA AutoMate software extension. Montaged images from INCA were post processed using FIJI software (Rasband, 2016). Micrographs were converted to single or stacked 8-bit tiff images using FIJI. Pore space areas were segmented by thresholding and noise was reduced by using tools to despeckle and removing outliers (radius 5.0 pixels/threshold 20%). Elemental maps were overlain on SEM-BSE images using FIJI or the INCA-Cameo function. Cameo was used to generate elemental maps where different hues in the image represent the acquired X-ray spectra from each element of interest.

3. OBSERVATIONS

3.1 FOAMED CEMENT ALTERATION

Foamed cement cylinders with different foam qualities, neat, 10%, 20%, and 30% gas volume, were exposed to SC-CO_2 at 50°C and 28.9 MPa for up to 56 days. Photographs of unreacted and reacted cores are shown in Figure 1.

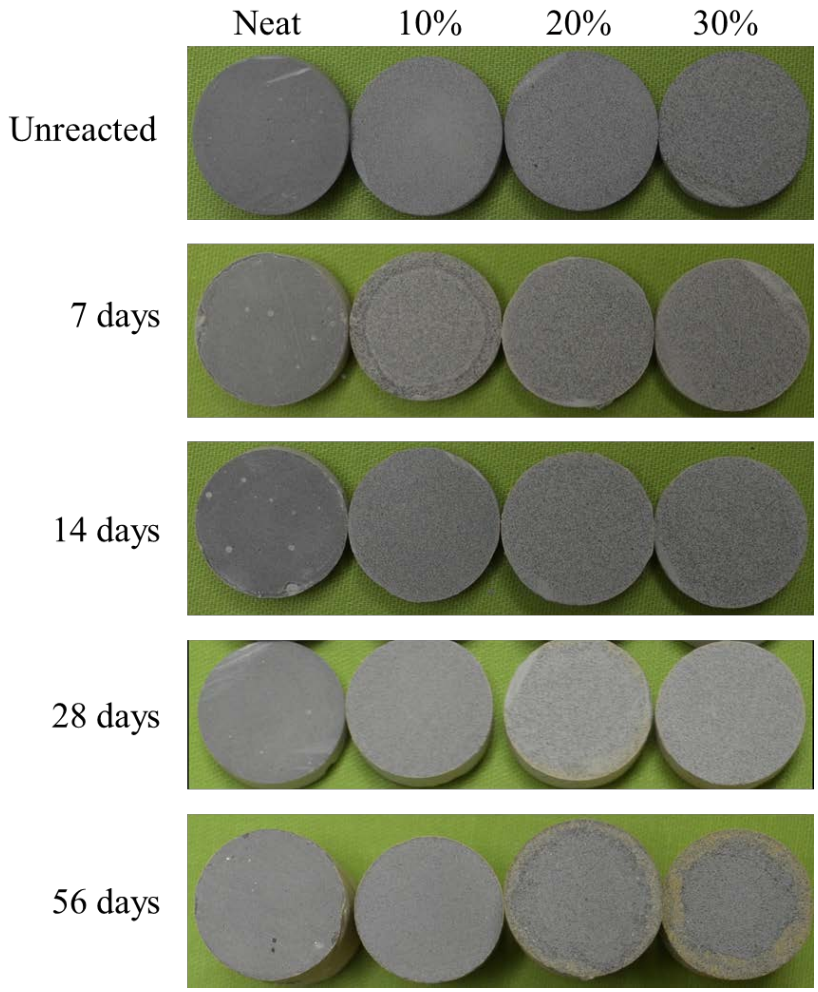

Figure 1: Photograph of 25.4-mm diameter samples cut from unreacted and reacted laboratory generated neat and foamed cement cores (bottom portion of core). Shown are the unreacted cores with different foam qualities (top row) and post reaction cores after 7, 14, 28, and 56 days (subsequent rows).

The alteration zones previously described by Kutchko et al. (2008) consisting of an outer amorphous silica zone, a well crystallized $CaCO_3$ band, and a Ca-depleted zone were observed to some degree in all samples in SEM observations (Figure 3). Based on the experimental work done here, the transport of CO_2 is controlled by diffusion and sorption; the foam quality appears to be a primary factor in controlling the carbonation depth of the cement. The local diffusivity is

dependent on the overall porosity and the geometry of the pore spaces (e.g. size, shape, connectivity). Ultimately, CO_2 sorption onto the pore walls appear to alter pore geometry and thus impact the total alteration. Neat cement has much smaller intergranular porosity and pore throats which limits the ingress of CO_2 molecules and subsequent carbonation reactions; the 30% foam quality had an increase in pore volume up to 47% (Table 3) which could facilitate more reactions. This is consistent with previous studies that found higher foam quality samples had larger void spaces and potentially higher permeability (e.g. Kutchko et al., 2013; Crandall et al., 2014; Glosser et al., 2016). Covariation of pore geometry with foam quality may be a driving factor in the diffusion of species in foamed cement, as well as the observed differences in alteration between foam qualities. The greater amount of surface area provided by the pore spaces in higher quality foams creates more surface area for both sorption and diffusivity of chemical species. Ultimately, this increased surface area provides more material for these cement carbonation reactions, and subsequent alteration of the samples; however, the matrix pores tend to be small and poorly connected. As such, void volume itself is not a primary control on alteration as the neat cement would also exhibit substantial alteration if this were the case.

Table 3: Measured properties of experimental neat and foamed cement after exposure to SC-CO_2 for 56 days with standard deviation (S.D.)

Cement Property	Neat	10%	20%	30%
Alteration Zone				
2D SEM Average total alteration depth (mm)	0.31±0.13	0.10±0.02	5.3±0.17	8.35±0.13
2D SEM Segmented alteration (% area)	0.15±0.08	0.004±0.001	20.2±0.23	34.6±0.19
CT Whole Core 3D Alteration Zone Volume (%)	6.48	25.78	43.18	46.11
CT Reacted (Blue in Figure 10)	6.48	17.25	26.75	18.2
CT Intermediate (Purple in Figure 10)	0.00	8.53	16.43	27.91
SEM Calculated Pore Space				
2D Segmented pore space, unreacted (% area)	0.30±0.13	0.22±0.03	2.54±0.07	7.91±0.0
2D Segmented pore space, reacted (% area)	0.57±0.05	0.23±0.09	2.51±0.09	5.76±0.2
Geomechanical				
Porosity (%)	19.51	30.84	43.25	47.02
Permeability (mD)	0.002	0.004	0.029	0.041

The scope of the study was to determine if the integrity of wells completed with foamed cement could be impacted by the injection of CO_2. The development and spatial spread of the CO_2-induced alteration is minimal in the neat cement sample as compared to total alteration in the 30% foamed cement sample (Table 3). The 30% sample has approximately 27 times more alteration as compared to the neat cement. The 20% foam quality had nearly 17 times the alteration of the neat cement sample. Conversely, the 10% foam quality displayed nearly comparable alteration to the neat sample with an average alteration of 0.10 ± 0.02 mm.

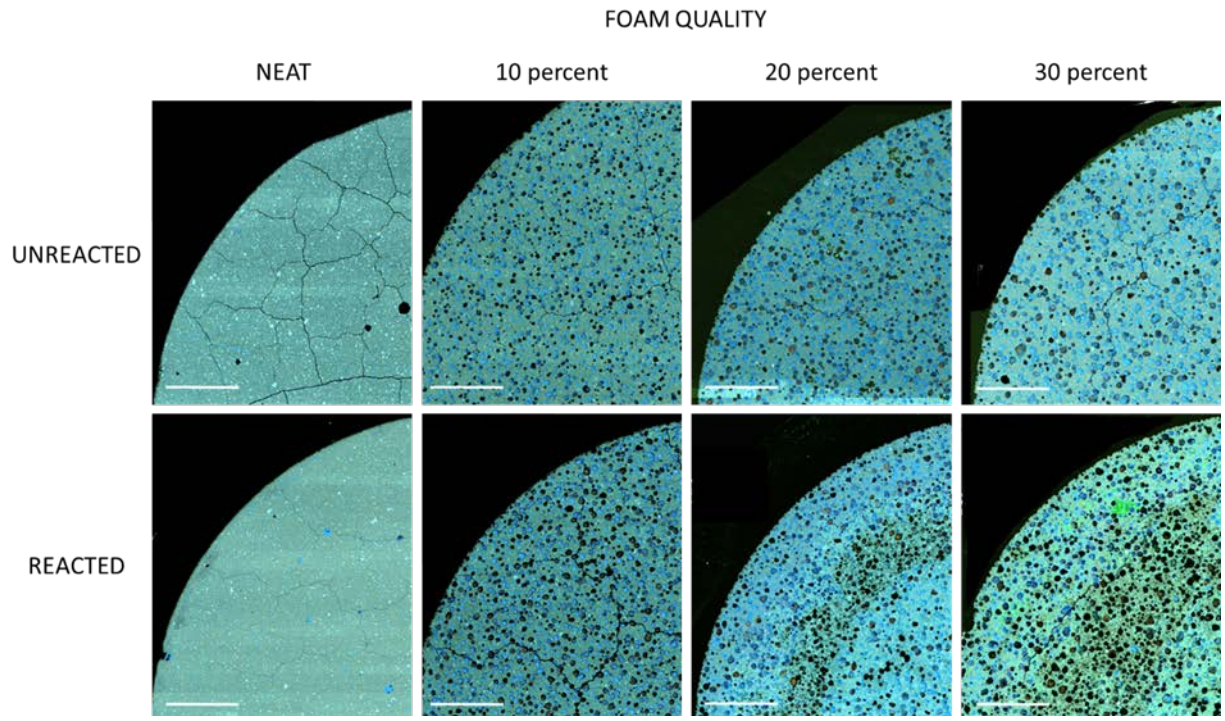

Figure 2: SEM backscatter image with of unreacted and reacted foamed cement of variable foam qualities (neat, 10%, 20%, and 30%) overlain with elemental maps [Ca- blue, Si green]. Scale bar is 3 mm. Cracks are likely due to sample prep.

The reaction of SC-CO_2 with the 30% foam quality cement resulted in the highest degree of alteration out of all the samples (Figure 2). Secondary mineralization is important to understand as it impacts the cement porosity and permeability of acidic fluid, and thus carbonation. A secondary mineral chemically consistent with (Mg,Ca)$CaCO_3$ formed at the edge of the carbonation front as magnesium (originally from MgO) was pushed into the sample. This reflects the stability of first vaterite, calcite, and then magnesite or dolomite.

SEM images of cement and pore spaces (10 and 20% foam quality) after 56-day exposure period (Figure 3, top and bottom left) show the alteration zone, cement matrix, and pore space. Empty pore space appears black and pores filled with secondary minerals appear in grey. Pore bubbles in the alteration zone are filled with various calcite polymorphs with a general composition of 9% Ca, 26% C and 65% O (atm %). The morphology of pore filling carbonates ranges from thin needles and cubes (top right) to euhedral crystals (bottom right). Secondary carbonate minerals (e.g., calcite and aragonite) are found in the pore spaces of all reacted foamed cement samples analyzed.

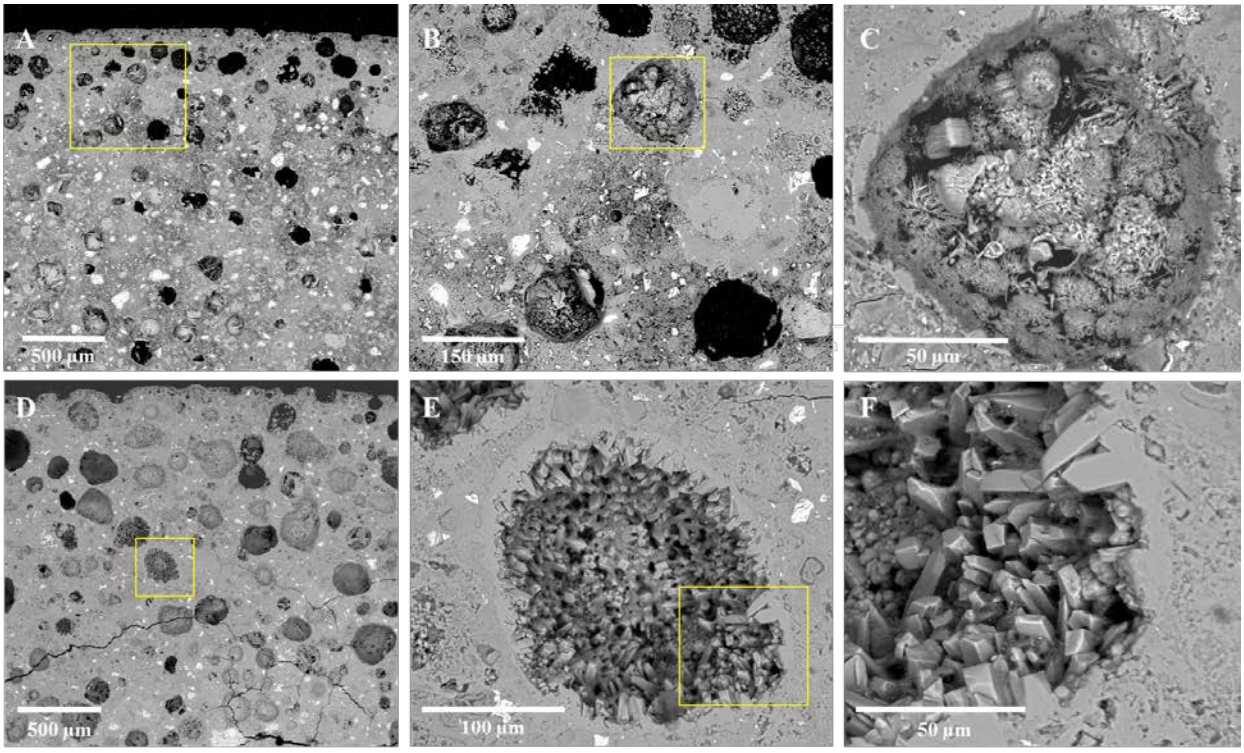

Figure 3: SEM images of reacted foamed cement samples with 10% (A–C) and 20% (D–F) foam quality exhibiting the changes in pore space.

The 10% foam quality sample showed evidence for alteration after 7 days (Figures 2 and 4). SEM images and elemental maps show the alteration zone and evidence for redistribution of Ca, Na, Si, and Cl along the outer edge of the cement core (Figure 4). Most obvious is the infiltration and segregation of Na and Cl into the reaction zone along the outer ~3 mm of the core. Elemental maps show the detrital outer silica rind as other cations are pulled into solution, carbonation zone, and a Ca-leached zone. The results shown in Figure 3 depict the transport and fate of ions from the brine solution into the cement and cement matrix. Further work on the diffusion and transport of ions into the cement matrix could help better resolve the fluid mechanics and ion partitions in the cement during initial contact between the cement and the fluid (e.g., subsurface brine or formation waters) during the initial stages of reaction. This could ultimately be important to modeling the transport of ions in and out of the cement matrix under different conditions.

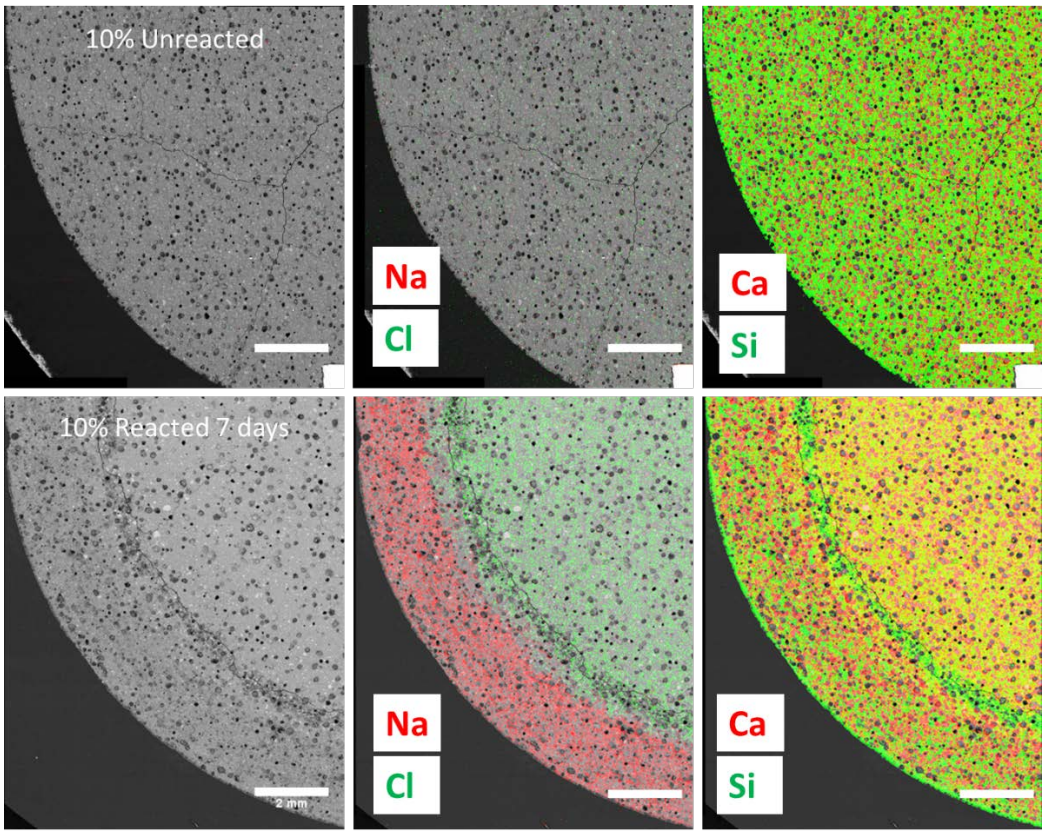

Figure 4: SEM images of 10% unreacted (top row) and 7-day reacted (bottom row) cement. Center and right images in each row show the distribution of Ca, Na, Si, and Cl in the cement.

This study also demonstrates that the presence of brine plays a role in the diffusion of chemical species into the cement matrix (Figure 5) and precipitation, specifically Friedel's salts ($Ca_2Al(OH)_6(Cl, OH)$ 2 H_2O) and halite (NaCl), in the 20% and 30% foam quality (Figure 4). Portland cement has chloride binding properties where chloride chemically bonds to the gel-like C-S-H during hydration of Ca_3SiO_6 (e.g. Beaudoin et al., 1990). SEM-EDS petrography showed the chloride bonding became more prominent after CO_2 injection. It appears that the cement continued to hydrate with time and that the bonded chloride provided sites to form micro-halite crystals. Halite formation may be attributed to experimental depressurization, although the kinetic rates are too rapid for halite to precipitate large crystals. In addition, Carey et al. (2007) documented the presence of salts in the wellbore in the Scurry Area Canyon Reef Operators Committee (SACROC) West Texas Enhanced Oil Recovery (EOR) operations and Pruess and Muller (2009) determined that the injection of CO_2 into saline aquifers may cause formation "dry-out" and precipitation of NaCl near the injection well.

The primary mechanisms may include brine displacement away from the injection well, dissolution/evaporation of brine into the injected CO_2 plume, upflow of CO_2 due to buoyancy effects, backflow of brine, and/or molecular diffusion of dissolved salt. This study expects that a similar mechanism may have contributed to the deposits of NaCl on the surface of the cement samples along with the continuation of cement hydration, dehydrating the cement pores. Halite precipitation requires higher dissolved salt concentrations in the pores than is available in the brine itself. Cement hydration would enable the solubility to increase in the pore space and allow

halite to precipitate. Fluid properties, parameters of displacement, and fraction of pore space must be considered; however, further studies are required to examine if salts impact wellbore integrity.

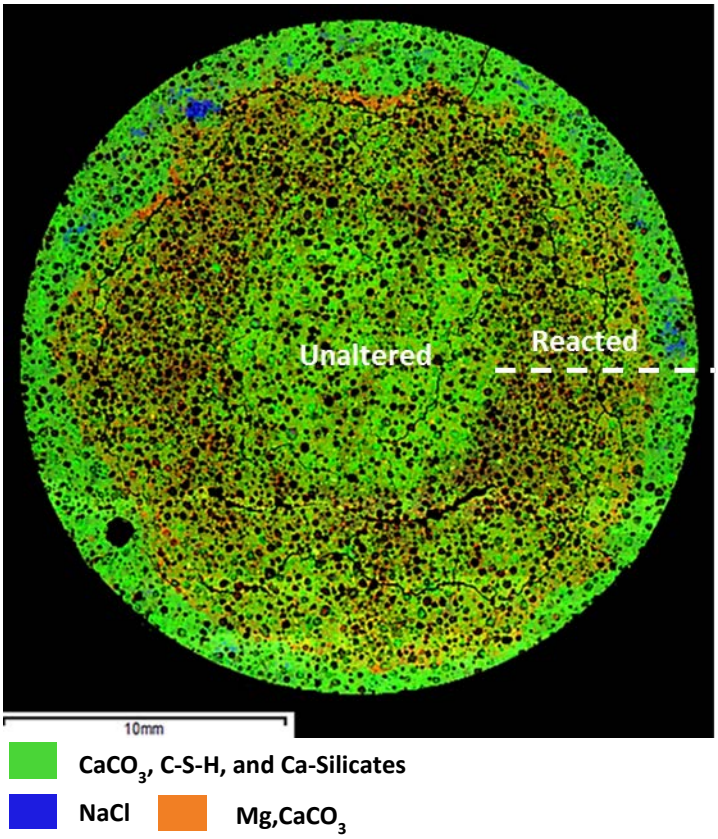

Figure 5: Qualitative SEM stitched cameo map showing the phase distribution of the 30% foam quality cement sample 56 days post-CO_2 injection. Colors are represented by blue = NaCl; orange= Mg, $CaCO_3$; and green= Ca-phases (e.g. $CaCaCO_3$, C-S-H, and calcium silicates).

Macroscopic measurements of the alteration area in samples exposed for 56 days were made. Figure 6 shows photographs of the 20 and 30% foam quality cement samples (left) and the post processing segmented area (right) used to calculate the total areal alteration. The alteration area was calculated for all samples (Table 3) though only the results for the 20 and 30% foam quality are shown. The area of alteration for the 20 and 30% foam quality samples was 20.2% and 34.6% respectively.

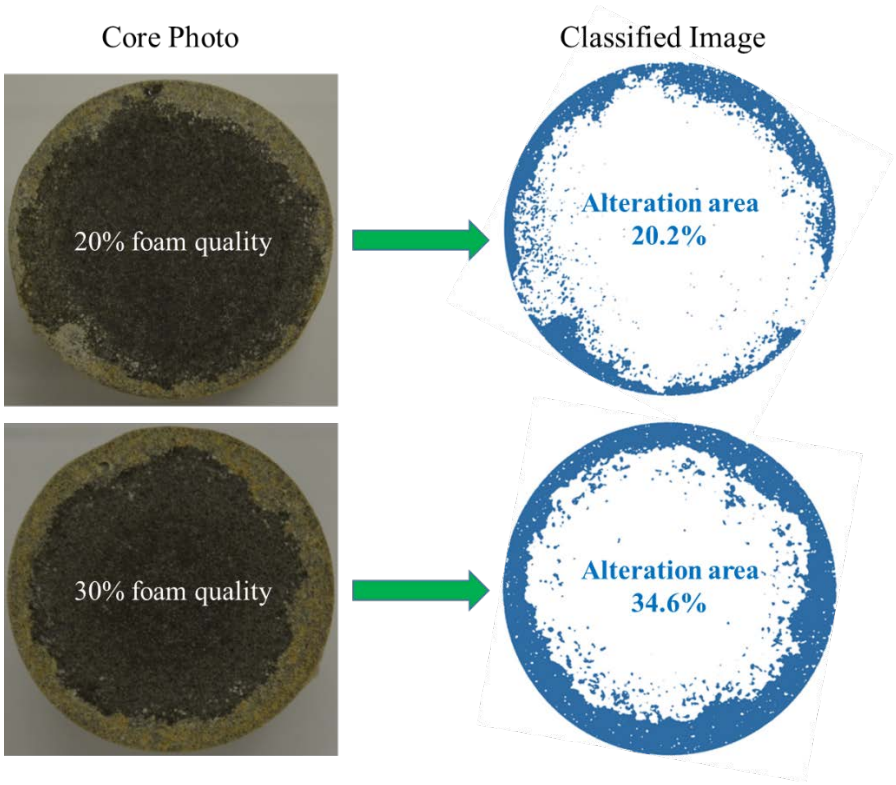

Figure 6: Image analysis of area of alteration zone using thresholding and segmentation and then quantified in the image program FIJI.

Montaged SEM images of unreacted controls and 56-day reacted samples were used to calculate the area and distribution of unfilled pore space in the samples. Figure 7 shows the results of 2D pore space segmentation for the 20 and 30% foam quality samples. The complete results are shown in Table 3. Pore space area in the samples remained relatively the same between the unreacted and reacted samples with neat, 10 and 20% foam quality. However, there was a 25% decrease in the pore area in the 30% foam samples reacted for 56 days. The segmentation results provide an image of how the distribution of unfilled pores changes after exposure to CO_2-NaCl. In the unreacted samples there is a fairly even distribution of unfilled pore spaces throughout the cement core. After reaction for 56 days, pore space is reduced in the alteration zone; pore space is more discrete and forms a concentric zone within the Ca leached zone of the cement.

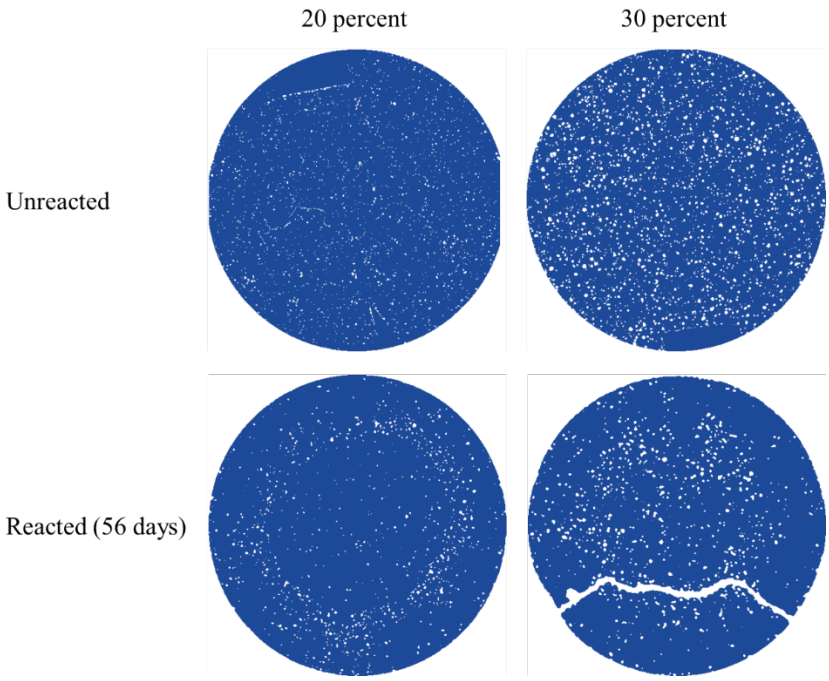

Figure 7: 2D segmentation of pore space (in white) in montaged SEM images comparing unreacted and reacted 20% and 30% foamed cement samples. The diameter of the cores is ~25.4 mm. The large fracture (in white) shown on the 30%, reacted core (bottom right) was not included in the final measurement of pore area.

3.2 COMPUTED TOMOGRAPHY OF WHOLE CORES

The 56-day reacted samples were scanned using NETL's North Star Imaging M-5000 industrial CT scanner to non-destructively obtain 3D digital representations of the cores with a voxel resolution of 15.2 microns. Each sample was scanned in five discrete sections to obtain this fidelity of imaging. After reconstructing the radiographs from scanning, each section was exported as a stack of approximately 1,800 2D 16-bit greyscale TIF images using North Star Imaging's EFX software with no beam hardening or other corrections applied to the images. The approximately 9,000 images per core were analyzed and combined with ImageJ (Rasband, 2106) and Ilastik (Sommer et al., 2011) to obtain the following insights.

An initial observation on the macroscopic variation of the reacted portion of the cement samples is shown in Figure 8, where the bottom of each sample was observed to have a larger reacted zone. The area of reacted cement is clearly visible in the greyscale images of Figure 8 for the 10, 20, and 30% samples as a light grey zone radiating into the core, adjacent to a ring of darker material. As was illustrated in Section 3.1, the zone adjacent to the edge of the core is assumed to be an amorphous silica zone while the darker band of material is a crystallized $CaCO_3$ band. CT imaging did not provide the level of detail to confirm this, but the associated SEM analysis presented does suggest this. Qualitatively, the volume of cement that has been reacted in the higher foam quality samples (20 and 30%) does appear greater in the cross-sections shown in Figure 8 as well.

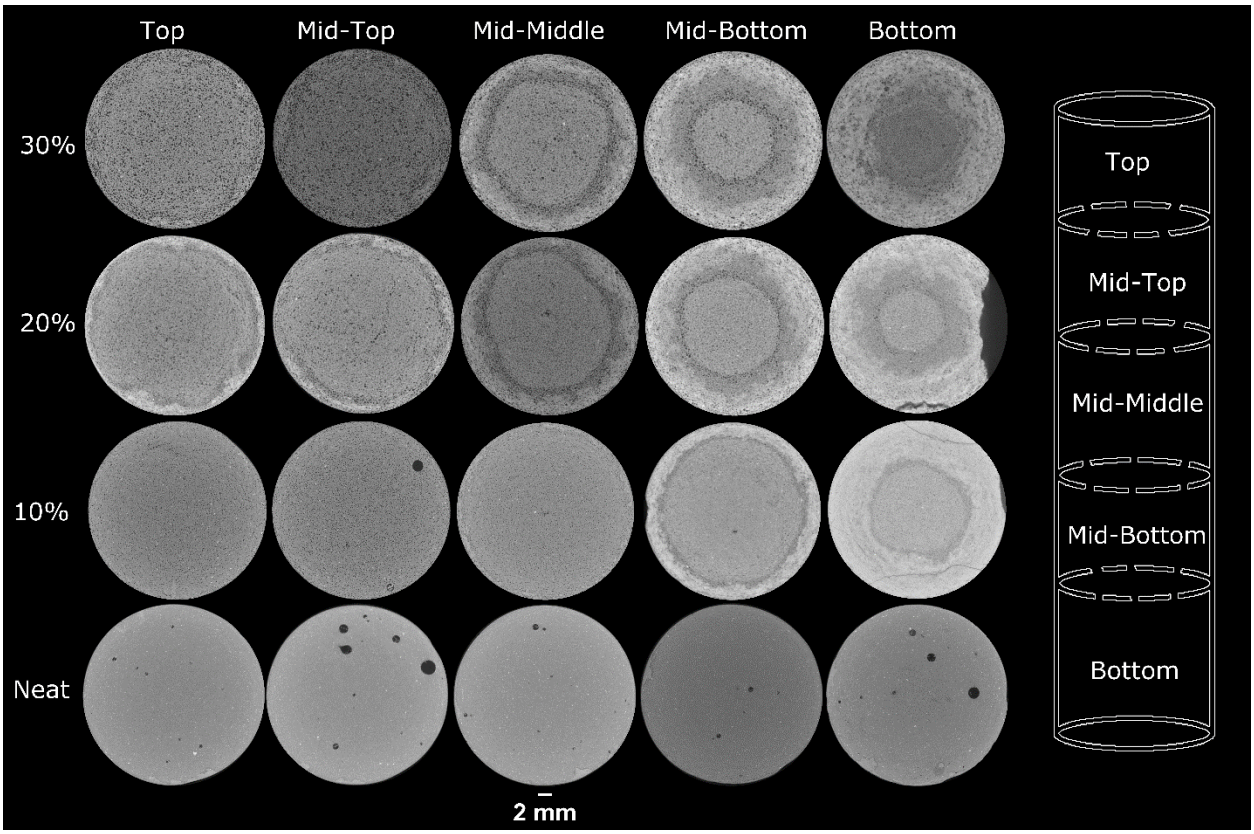

Figure 8: CT montage: XY view of each core section after 56 days of exposure for neat, 10%, 20%, and 30% cores.

By stitching together the approximately 9,000 2D images associated with the full scan of these cores, the mid-plane of the cores can be visualized and is shown in Figure 9. These are labeled as planes through the core in the XZ direction, assuming Z is along the length of the core. Slight variations in the greyscale can be observed due to slightly different atmospheric and material properties of each section scanned; these have been compensated for by contrast and brightness modifications in ImageJ (Rasband, 2016) to provide a qualitative view of the reacted zones within the sample. The reacted zone at the base of the 10, 20, and 30% foamed cement samples are shown to have experienced a significantly greater amount of alteration due to CO_2/brine exposure than the top of these samples, suggesting that the tops of the samples were in a SC-CO_2 environment as opposed to a SC-CO_2/brine environment; this difference in reaction penetration rate and mechanisms are well described in Kutchko et al. (2011). In addition, the increase in penetration of the reaction within the higher quality (20 and 30%) cement samples are clear from these cross-sectional views.

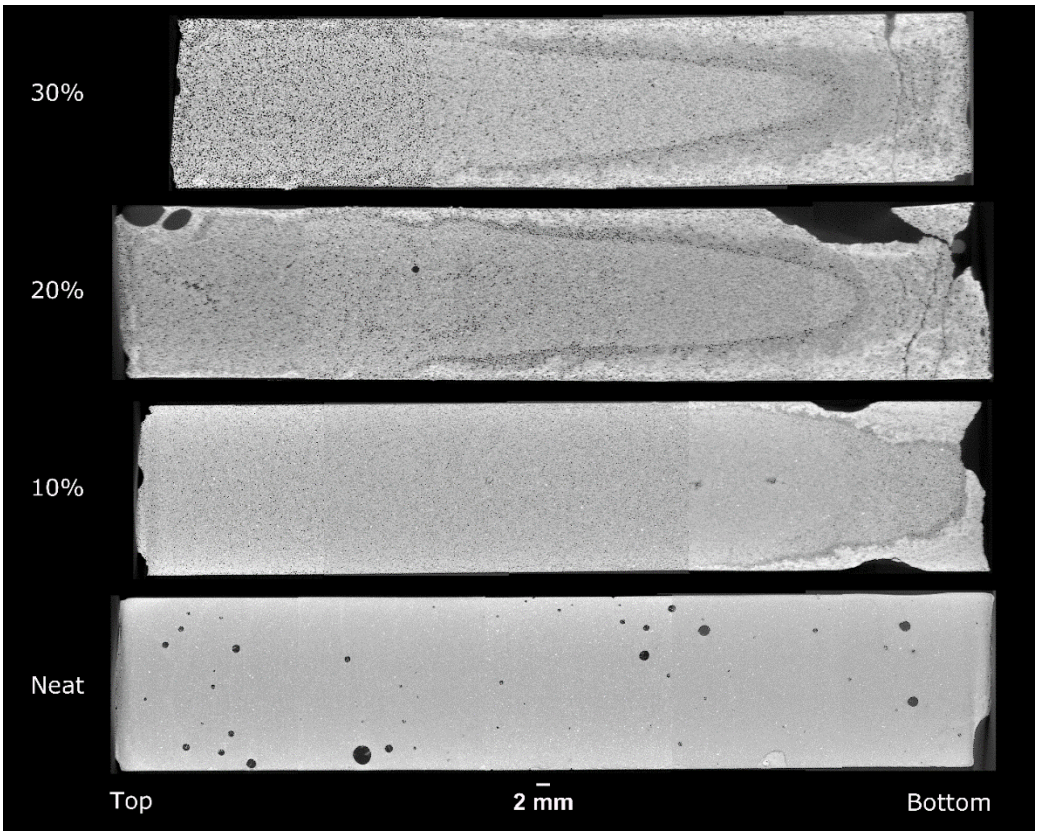

Figure 9: Stitched CT core montage on the XZ direction for neat, 10%, 20% and 30% cores.

Quantitative measurement of the reacted volume from the CT images is difficult and subjective to image processing. To reduce the subjectivity of manual isolation of features, the thresholding program Ilastik (Sommer et al., 2011) was used to train machine learning algorithms to isolate and segment the reacted zones from the 3D volume. A 300 slice (4.56-mm thick) cylinder in the center of the "mid-bottom" scan (see Figure 8) was selected for each sample. Each of these sections are shown in Figure 10 with the total reacted volume highlighted. The light blue reacted zones on the outside of the core is segmented from the intermediate zone as well. The neat cement had no intermediate reacted zone, discernable at the resolution of the CT scans, at the location measured. These reacted volumes were summed and are presented in Table 3. The total altered volume encompassed 46% of the volume for the 30% foam quality cement, with a similar percentage of reacted volume (43%) measured in the 20% foam quality sample. The 10% quality sample had only 26% reacted volume and the neat cement only has a small reaction rind comprising 6.5% of the cement volume. The relatively similar, and large, volume of reacted cement observed in the 20 and 30% foam quality samples suggest that above a certain gas fraction the SC-CO_2/brine is able to penetrate into the cement volume more readily. The lower amount of reacted cement observed in the 10% and neat samples suggest that the matrix porosity, with much smaller gas voids, restricts fluid invasion into the cement and highly restricts the penetration of the reaction front.

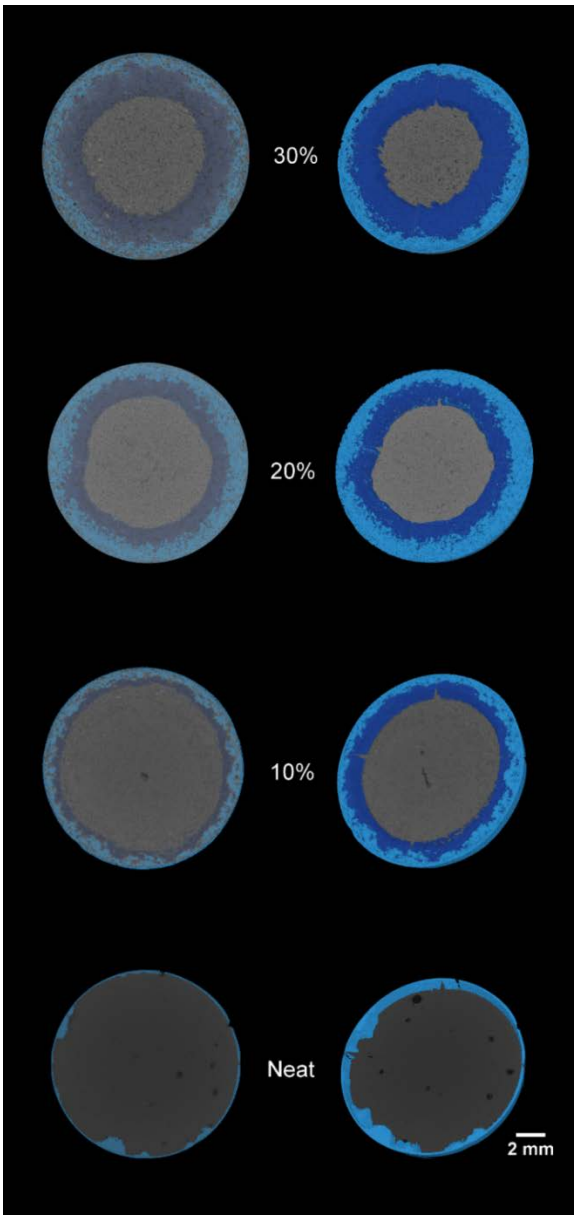

Figure 10: CT segmented 3D front and angled views of alteration zone.

To further illustrate the influence of larger voids enabling fluid penetration into the matrix, several slices of the 20% quality sample, after 56 days of exposure are shown in Figure 11. As was shown in Figure 9 (XZ cross-sections of the core) some larger voids within the cement matrix existed near the top of the sample and adjacent to the edge of the core. These large voids appear to have enabled the SC-CO_2 reaction to penetrate further into the core. Slices though the entire core are shown in Figure 11 that are approximately 3 mm apart, starting from the left, above the large void features, and bisecting the voids and reacted zones. The lighter grey reacted zone is observed to be a narrow rind on the outside of the core far away from the large voids, but then penetrates farther into the matrix surrounding the open areas. This ability of the external fluid to more readily interact with the cement due to migration pathways created by the voids is

likely the reason the higher quality samples exhibited a larger reacted volume, and is shown here on a larger scale visible via CT scanning.

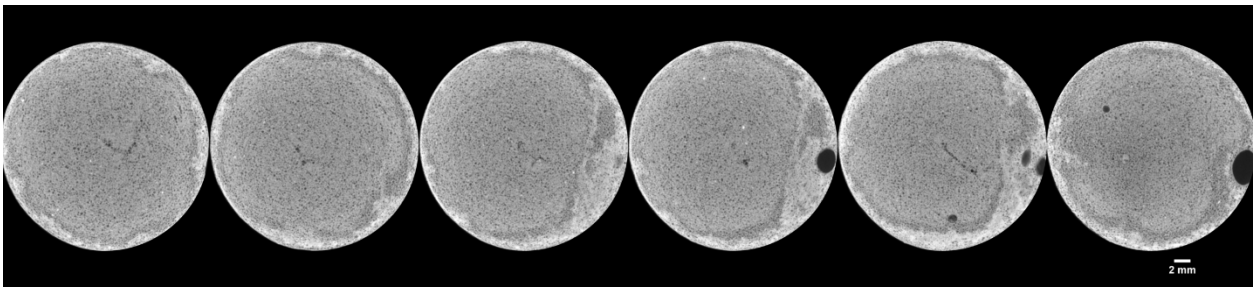

Figure 11: XY slices of the 20% quality sample after 56-day exposure with large void in cement.

3.3 PHYSICAL AND GEOMECHANICAL RESULTS AND OBSERVATIONS

The physical characteristics of the unreacted samples show that both permeability and porosity values increase with foam quality (Table 4). This result was expected based on previous work (Kutchko et al., 2014; Spaulding, 2015) and ensures sample quality. However, upon exposure to SC-CO_2, this correlation no longer is valid (Table 5). All samples, except for the 30% foam quality, become slightly less permeable after 7 days of being exposed to SC-CO_2 (Figure 12). This could be the result of having a larger surface area to be affected by the CO_2 attacking the cement as mentioned earlier (Section 1.2). After 14 days of exposure, all of the samples became less permeable once again, this time including the 30%. This may be the result of mineral precipitation in the connected pore throats, thereby closing the flow pathway and lowering the values. However, when looking at the 28-day exposed cements, the permeability of the neat, 20%, and 30% all increase. For the 56-day exposure, the permeability of the neat, 10%, and 30% decrease while the 20% increases slightly. The erratic nature of these values over the course of the experiment can conceivably be attributed to several possibilities: the nature of the precipitation/dissolution events that occur during the carbonation and/or bicarbonation process, or due to fluctuations within the error of the machine used for testing. It is important to note that all measurements are based off of a single post reacted sample; the unreacted samples were averaged from two measurements per sample. Further experiments and measurements are forthcoming to determine the statistical accuracy of these measurements. However, given the excellent correlation between the “pre-exposed” cement samples and the previous work generated using the same foam qualities (Spaulding et al., 2015; Kutchko et al., 2015), there is a measure of confidence in these results.

Table 4: Unreacted cement samples physical and mechanical properties with the averages highlighted

Sample	Porosity (%)	Bulk Density (g/cc)	Permeability (mD)	Young's Modulus (GPa)	Poisson's ratio
CO_2-F-N-0-1	22.5	1.77	0.00271	20.0	0.208
CO_2-F-N-0-2	23.4	1.75	0.00478	19.6	0.201
NEAT Averages	**23.0**	**1.76**	**0.00374**	**19.8**	**0.204**
CO_2-F-10-0-1	43.4	1.33	0.0199	9.56	0.188
CO_2-F-10-0-2	40.8	1.39	0.00919	10.8	0.193
10% Averages	**42.1**	**1.36**	**0.0146**	**10.2**	**0.191**
CO_2-F-20-0-1	46.3	1.24	0.0143	8.82	0.196
CO_2-F-20-0-2	49.0	1.17	0.0408	7.56	0.185
20% Averages	**47.7**	**1.20**	**0.0276**	**8.19**	**0.190**
CO2-F-30-0-1	50.4	1.14	0.0252	7.52	0.202
CO2-F-30-0-2	51.2	1.12	0.0623	6.97	0.188
30% Averages	**50.8**	**1.13**	**0.0438**	**7.25**	**0.195**

Table 5: Reacted cement samples physical and mechanical properties. Sample identification is annotated by CO_2 foamed cement; foam quality; duration. Samples that broke and measurements for Young's modulus and Poisson's ratio are highlighted.

Sample	Porosity (%)	Bulk Density (g/cc)	Permeability (mD)	Young's Modulus (GPa)	Poisson's ratio
CO_2-F-N-7	22.1	1.79	0.00579	19.9	0.212
CO_2-F-10-7	37.6	1.47	0.0102	12.4	0.208
CO_2-F-20-7	**45.0**	**1.28**	**0.0221**	**No Data**	
CO_2-F-30-7	51.5	1.67	0.0646	10.8	0.183
CO_2-F-N-14	21.0	1.79	0.00313	20.8	0.217
CO_2-F-10-14	39.7	1.42	0.00893	12.0	0.209
CO_2-F-20-14	47.8	1.24	0.0195	9.06	0.193
CO_2-F-30-14	50.6	1.18	0.0593	7.92	0.190
CO_2-F-N-28	**21.3**	**1.82**	**0.00370**	**No Data**	
CO_2-F-10-28	35.4	1.52	0.00850	13.5	0.209
CO_2-F-20-28	46.2	1.29	0.0284	9.84	0.207
CO_2-F-30-28	50.5	1.20	0.0911	7.86	0.165
CO_2-F-N-56	19.5	1.81	0.00190	20.5	0.221
CO_2-F-10-56	**30.8**	**1.51**	**0.00419**	**No Data**	
CO_2-F-20-56	43.2	1.31	0.0289	9.84	0.205
CO_2-F-30-56	47.0	1.25	0.0415	8.57	0.172

The permeability of the cement exposed to SC-CO_2 for 56 days decreased by 5.2, 71.22, and 49.22% for foam qualities of 30%, 10%, and neat respectively. The 20% foam quality sample had an increase of 4.71%. The increase in the 20% or the significant decrease in the 10% will require further study to determine if these are statistical changes.

The overall porosity trends show a more stable array of measurements over the entire exposure time. The samples in this study showed that porosity decreases over the length of the experiment for each foam quality. The porosity for the foamed cements decreases by 7.42%, 9.37%, 26.75%, and 15.03% for the 30%, 20%, 10%, and neat cement, respectively (Figure 12). Additional porosity measurements will be forthcoming in the future for a more robust dataset.

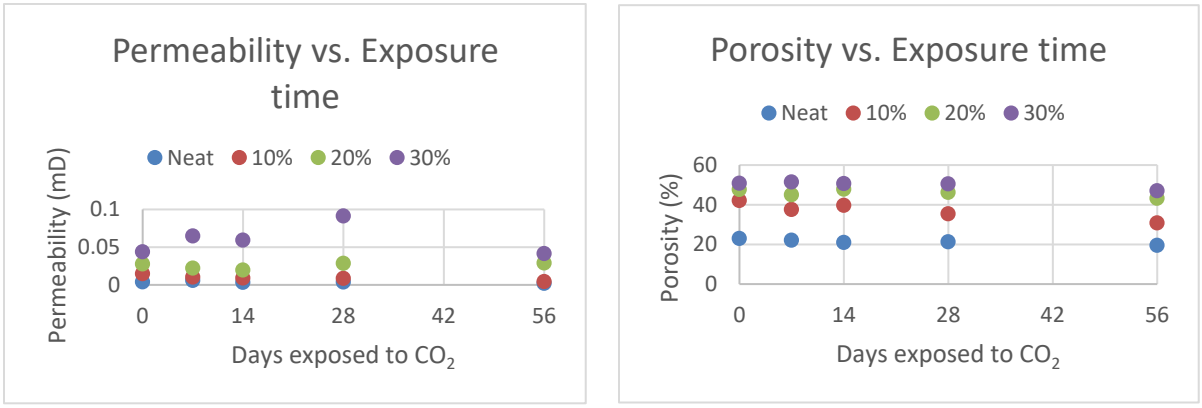

Figure 12: Permeability and porosity measurements of neat, 10%, 20%, and 30% foam quality cement over a period of exposure time.

The mechanical characteristics of these cements show little definitive information. Young's modulus is a measure of the stiffness of a material (i.e. how brittle or ductile a material is); a higher Young's modulus indicates a more brittle material, whereas a lower Young's modulus describes a more ductile material. Young's modulus can be used to predict the elongation or compression of a material (Craig, 2011). The unreacted cement samples show a decrease in Young's modulus with increasing amounts of entrained air (foam quality). This is consistent with previous studies (Spaulding et al., 2015; Kutchko et al., 2015). Comparatively, the Young's modulus for all reacted samples increased slightly over the course of the 56 days of SC-CO_2 exposure: the neat, 20%, and 30% increased roughly 3.48%, 20.29%, and 18.34% respectively (Figure 13; Appendix Tables A1, A2). The 10% shows an increase of roughly 32.35% after 28 days; however, after exposure for 56 days to CO_2 the 10% foam quality sample experienced a complete loss of structural integrity during the PDP measurements, so no mechanical property measurements were able to be recorded in AutoLab. This loss of integrity also occurred to the 20% exposed for 7 days and the neat cement exposed for 28 days.

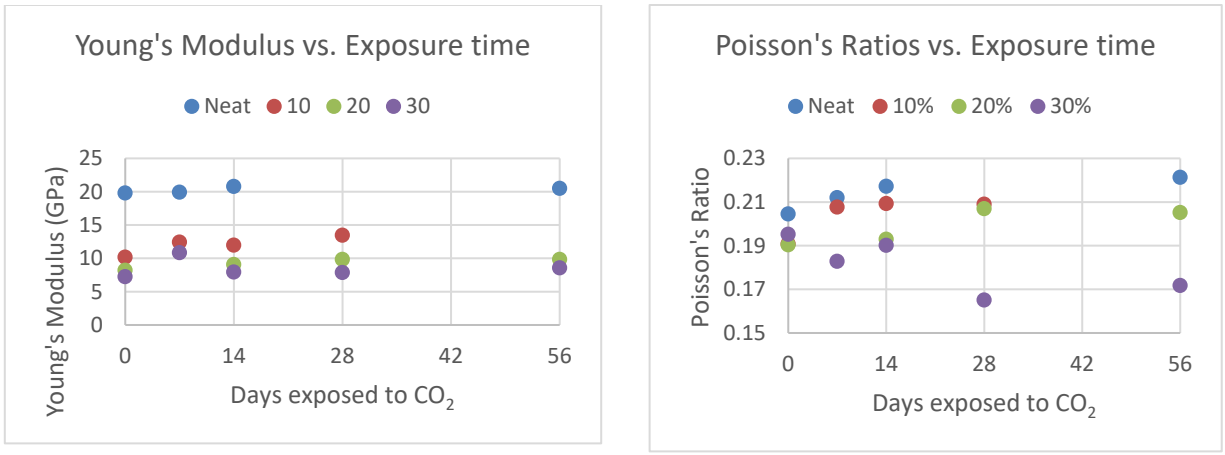

Figure 13: Young's module and Poisson's ratio measurements of neat, 10%, 20%, and 30% foam quality cement over varying periods of exposure time.

Previous experiments have shown that Young's modulus has a linear relationship with compressive strength (Spaulding et al., 2015). However, compressive strength tests have not yet been conducted on these samples. As mentioned above, some of the samples lost their structural integrity when placed under a confining pressure of roughly 3.89 MPa in the PDP core holder (annotated in Appendix Table A2). Several of the reacted samples lost their structural integrity within the AutoLab, either during measurements or during depressurization, where the stress may have exceeded the longitudinal strain. It appears that the area most likely to fail during these mechanical tests is very similar to the reaction rings shown earlier in this paper; this is likely due to differences in the material property interface creating a zone of structural weakness.

During the compression of a material in one direction, expansion may occur perpendicular to the direction of the compression. This occurrence is known as the Poisson effect and is measured by Poisson's ratio. Poisson's ratio is the negative ratio of transverse to axial strain (Craig, 2011). Most isotropic materials have Poisson's ratio values ranging between 0.0 and 0.5. The less compressible the material, the higher the Poisson's ratio—a material with a Poisson's ratio of 0.5 is considered incompressible. Conventional cements have a Poisson's ratio of about 0.15 (Nelson, 2006). Poisson's ratio is consistent for all unreacted foam qualities and is similar to that of the neat cement. When looking at the reacted cements, all foam qualities but the 30% increase in lateral strain with exposure time. When compared to the unreacted cement samples, the 56-day exposed neat and the 20% had an increase of 8.2 and 7.7% respectively. While the 10% was unable to be measured at 56-day exposure, it still showed an increase in Poisson's ratio by about 9.5% by 28 days of exposure. The 30% foam quality appears to have a decrease in Poisson's ratio by about 12% (Figure 13). This suggests that while being exposed to SC-CO_2, the 30% foam quality cement becomes less likely to expand perpendicularly when compressed while the other qualities are more prone to this expansion. Attempts to correlate the physical and mechanical data over the exposure times have proven to be difficult (Appendix Tables A3–A4). In terms of the Poisson's ratio with time, there appears to be a moderate correlation (0.55–0.70) while porosity with time has a moderate to strong correlation (0.57–0.90). Young's modulus with time has a weak correlation of the neat and 30% cement (0.29 and 0.001), whereas the 10% and 20% have moderate correlation (0.77 and 0.74). The permeability followed a similar trend to the variability seen in Young's modulus values where the neat and 10% had moderate to strong

correlation (0.51 and 0.85), whereas the 20% and 30% had weak correlation (0.24 and 0.007). However, more data points are required to be able to correlate these parameters with confidence.

Further studies should be undertaken to see how much the CO_2 exposure time can affect the compressive strength of these types of foamed cements. As it stands now, the geomechanical data presented in this paper shows that the 30% foam quality is the most likely to be affected by CO_2 storage techniques. However, more testing is necessary to determine just what the extent this effect will have on the wellbore stability and integrity.

3.4 CONCLUSIONS

The primary mechanism of cement carbonation and alteration under supercritical CO_2 conditions has been previously studied and the majority of publications conclude that the transport of CO_2 is controlled by diffusion and sorption. However, this is the first study in which foamed cement was studied in a supercritical CO_2 environment. Foamed cement is significant in that it is commonly used in the Gulf of Mexico and that the microstructure (e.g. BSD) could highly impact the rate of diffusion and sorption. This study shows that the overall foam quality plays a role in the degree of alteration and is most likely mediated by intra-foam quality differences in pore size and structure, both initially and subsequent to exposure to SC-CO_2 conditions. It is important to note that all of these results were based on atmospheric-generated foamed cements.

- For atmospheric-generated foamed cements, the higher quality foamed cements (i.e. 20% and 30%) tend to have larger initial pore sizes and greater interconnectivity than the lower quality foams (i.e. neat and 10%). This results in more cement material initially available for reactivity with the CO_2.
- Subsequent to exposure, higher foam quality cements displayed a greater degree of alteration as compared to lower foam quality cements. The alteration zones consist of an outer amorphous silica zone, a well crystallized $CaCO_3$ band, and a Ca-depleted zone which were observed to some degree in all samples in SEM observations. This mechanism of alteration is consistent with other studies.
- Total alteration depths in the neat, 10%, 20% and 30% samples were 0.31, 0.10, 5.39, and 8.35 mm respectively.
- Ultimately, CO_2 sorption onto the pore walls appears to alter pore geometry and thus impacts the total alteration area. Following 56-day exposure, the 30% foam quality cement showed a 25% decrease in pore area and is the most discrete in the alteration zone. The change in pore area is a result of secondary mineralization in these samples, which is evidence that the initial pore structure in these samples influences the degree of alteration by way of providing more cement material for these geochemical transformations.
- Potential next steps:
    - Modeling at supercritical CO_2 well conditions and determining how the model compares to experimental studies at pore level or continuum-scale.
    - Experimental: 1) A short term experiment (within the first 7 days of exposure) to better constrain the initial fluid movement with respect to the original unaltered pore connectivity; 2) Long term exposure cement for 6 months or 1 year.

4. REFERENCES

Anderson, S.; Newell, R. Prospects for Carbon Capture and Storage Technologies. *Annual Review of Environment and Resources* **2004,** *29*, 109–142.

API. American Petroleum Institute Standard 65-Part 2 Isolating Potential Flow Zones During Well Construction, December 2010.

API. American Petroleum Institute Standard recommended practice 10B, Washington, DC, 1997.

Bamforth, P. B. Spreadsheet model for reinforcement corrosion in structures exposed to chlorides. In *Concrete Under Severe Condition*, 2nd Ed.; Gjørv, O. E., Sakai, K., Banthia, N.; E&FN Spon: London, 1998; pp 64–75.

Barlet-Gouedard, V.; James S.; Drochon B.; Piot B.; Jean-Philippe C. Cement composition for carbon dioxide supercritical environment. US Patent 8,901,642 B2, 2012.

Beaudoin, J. J.; Ramachandran, V. S.; Feldman, R. F. Interaction of chloride and C-S-H. *Cement and Concrete Research* **1990,** *20*, 833–875.

Benge, G.; McDermott, J. R.; Langlinais, J. C.; Griffith, J. E. Foamed Cement Job successful in deep HTHP offshore well. *Oil and Gas Journal* **1996,** *94*, 58–63.

Benge, G.; Poole, D. Use of foamed cement in deep water Angola. Society of Petroleum Engineers. Presented at the SPE/IADC Drilling Conference held in Amsterdam, Netherlands, Feb 23–25, 2005; SPE/IADC 91662.

Benson, S. M.; Surles, T. Carbon dioxide capture and storage: An overview with emphasis on capture and storage in deep geological formations. *Proceedings of the IEEE* **2006,** *94*, 1795–1804.

Boukhelifa, L.; Moroni, N.; James, S. G.; Le Roy-Delage, S.; Thiercelin, M. J.; Lemaire, G. Evaluation of Cement Systems for Oil and Gas Well Zonal Isolation in a Full-Scale Annular Geometry. IADC/SPE Drilling Conference, Dallas, TX, March 2–4, 2004; SPE paper 87195.

Brady, K. C.; Watts, G. R. A.; Jones, M. R. *Specification for foamed concrete*; Project Report PR/IS/40/01; TRL Limited: Crowthorne Berkshire, England, 2001.

Carey, J. W.; Wigand, M.; Chipera, S. J.; WoldeGabriel, G.; Pawar, R.; Lichtner, P. C.; Guthrie, G. D. Analysis and performance of oil well cement with 30 years of CO_2 exposure from the SACROC Unit, West Texas, USA. *International Journal of Greenhouse Gas Control* **2007,** *1*, 75–85.

Chen, D.P.; Liu, J. Y.; Liu, M. Accelerated Carbonation Curing of Foam Concrete with Lower Density. *Advanced materials Research* **2011,** *250–253*, 172–177.

Craig, R. *Mechanics of Materials*, 3rd Ed.; Wiley, New York, 2011.

Crandall, D.; Gill, M.; Moore, J.; Kutchko, B. Foamed Cement Analysis with Computed Tomography. ASME 2014 4th Joint US-European Fluids Engineering Division Summer Meeting. 2014; Paper No. FEDSM2014-21589, pp. V01CT25A002.

De Beer, M.; Maina, J. Some fundamental definitions of the elastic parameters for homogeneous isotropic linear elastic materials in pavement design and analysis. Proceedings of the 27th Southern African Transport Conference; Pretoria: Document Transformation Technologies, 2008; 282–293.

De Rozieres, J.; Ferriere, R. Foamed-Cement Characterization Under Downhole Conditions and Its Impact on Job Design. *SPE Production Engineering* **1991,** *6*, 297–304.

Dhir, R. K.; Jones, M. R. Development of Structural grade Foamed Concrete; Final Report; DETR Research Project; University of Dundee, Scotland, 1999.

Dusterhoft, D. M. *A Comparison Between Foamed and Lightweight Cements*; Petroleum Society of Canada. 2003. DOI:10.2118/2003-125

Frisch, G. J.; Graham, W. L.; Griffith, J. Assessment of foamed-cement slurries using conventional cement evaluation logs and improved interpretation methods. SPE Rocky Mountain Regional Meeting, Gillette, Wyoming, May 15–18, 1999; SPE 55649.

Galiana, C.; Montaron, B.; Sherwood, R.; Vidick, B. Cement Mixing: Better Understanding and New Hardware. *Reprinted from Oilfield Review* **1991,** *3*, 11–21.

Gasda, S.; Celia, M.; Wang, J.; Duguid, A. Wellbore Permeability Estimates from Vertical Interference Testing of Existing Wells. *Energy Procedia* **2013,** *37*, 5673–5680

Gibbins, J.; Chalmers, H. Carbon capture and storage. *Energy Policy* **2008,** *36*, 4317–4322.

Gill, M.; Moore, J.; Crandall, D.; Kutchko, B. Analysis of Atmospherically Generated Foamed Cements using Computed Tomography. 6th International Conference on Porous Media & Annual Meeting of the International Society for Porous Media, Milwaukee, WI, 2014.

Glosser, D.; Kutchko, B.; Benge, G.; Crandall, D.; Ley, M. T. Relationship between Operational Variables, Fundamental Physics and Foamed Cement Properties in Lab and Field Generated Foamed Cement Slurries. *Journal of Petroleum Science and Engineering* **2016,** *145*, 66–76.

Griffith, J. E.; Lende, G.; Ravi, K., Saasen, A.; Nødland, N. E.; Jordal, O. H. Foam Cement Engineering and Implementation for Cement Sheath Integrity at High Temperature and High Pressure. Society of Petroleum Engineers, 2004. DOI:10.2118/87194-MS

Harlan, T. D.; Foreman, J.; Reed, S.; Griffith, J. Foamed Cement Selection for Horizontal Liners Proves Effective for Zonal Isolation—Case History. Presented at the 2001 Rocky Mountain Petroleum Conference held in Keystone, CO, May 21–23, 2001; SPE 71055.

Harms, W. M.; Febus, J. S. Cementing of fragile-formation wells with foamed cement slurries. *Journal of Petroleum Technology* **1985,** *37*, 1049–1057.

Holloway, S. An Overview of the Underground Disposal of Carbon Dioxide. *Energy Conversion and Management* **1997,** *38*, S193–S198.

Huerta, N. J.; Hesse, M. A.; Bryant, S. L.; Strazisar, B. R.; Lopano, C. L. Experimental evidence for self-limiting reactive flow through a fractured cement core: Implications for time-dependent wellbore leakage. *Environ. Sci. Technol.* **2013,** *47*, 269–275.

Huerta, N.; Hesse, M.; Bryant, S.; Strazisar, B.; Lopano, C. Reactive transport of CO_2-saturated water in a cement fracture: Application to wellbore leakage during geologic CO_2 storage. *Int. J. Greenh. Gas Con.* **2016,** *44*, 276–289.

IPCC. Climate Change 2007: Impacts, adaption, and vulnerability. Contribution of Working Group II to the fourth Assessment Report of the Intergovernmental Panel on Climate Change, Cambridge University Press, Cambridge, UK, 2007; 976.

Iverson, B.; Darbe, R.; McMechan, D. Evaluation of Mechanical Properties of Cements. American Rock Mechanics Association. Presented at the 42nd US Rock Mechanics Symposium and 2nd U.S.-Canada Rock Mechanics Symposium, San Francisco, 2008; ARMA 08-293.

Jones, M. R.; McCarthy, A. Preliminary views on the potential of foamed concrete as a structural material. *Mag Concr Res.* **2005,** *57*, 21–31.

Kopp, K.; Reed, S.; Foreman, J.; Carty, B.; and Griffith, J. Foamed Cement vs. Conventional Cement for Zonal Isolation-Case Histories. Society of Petroleum Engineers. Presented at the 2000 SPE Annual Technical Conference and Exhibition held in Dallas, TX, Oct 1–4, 2000; SPE 62895.

Kutchko, B. G.; Strazisar, B. R.; Huerta, N.; Lowry, G. V.; Dzombak, D. A.; Thaulow, N. CO_2 reaction with hydrated Class H well cement under geologic sequestration conditions: effects of flyash admixtures. *Environ. Sci. Technol.* **2009,** *43*, 3947–3952.

Kutchko, B. G.; Strazisar, B. R.; Lowry, G. V.; Dzombak, D. A.; Thaulow, N. Rate of CO_2 attack on hydrated class H well cement under geologic sequestration conditions. *Environ. Sci. Technol.* **2008,** *42*, 6237–6242.

Kutchko, B.; Crandall, D.; Gill, M.; McIntyre, D.; Spaulding, R.; Strazisar, B.; Gardner, C. *Computed Tomography and Statistical Analysis of Bubble Size Distributions in Atmospheric-Generated Foamed Cement*; NETL-TRS-2-2013, NETL Technical Report Series, U.S. Department of Energy, National Energy Technology Laboratory, 2013.

Kutchko, B.; Crandall, D.; Moore, J.; Gieger, C.; Gill, M.; Haljasmaa, I.; Spaulding, R.; Harbert, W.; Mergaman, A.; Dalton, A.; Rosenbaum, E.; Mcintyre, D.; Benge, G.; Buford, C.; Shine, J. Assessment of Pressurized Foamed Cement Used in Deep Offshore Wells. Offshore Technology Conference, 2015; OTC-25994-MS.

Kutchko, B.; Crandall, D.; Moore, J.; Gill, M.; Haljasmaa, I.; Spaulding, R.; Shine, J. *Assessment of Foamed Cement Used in Deep Offshore Wells*; Society of Petroleum Engineers, 2014; SPE 170298.

Kutchko, B.; Strazisar, B.; Hawthorn S.; Lopano, C.; Miller, D.; Hakala, A.; Guthrie, G. H_2S-CO_2 reaction with hydrated class H well cement: Acid-gas injection and CO_2 co-sequestration. *Environ. Sci. Technol.* **2011,** *5*, 880–888.

Mindness S.; Young J. F.; Darwin, D. *Concrete*, 2nd Ed.; Prentice Hall: Englewood CI, 1981.

Mueller, D.; Eid, R. Characterizing early-state physical properties, mechanical behavior of cement designs. *Drilling Contractor* 2006.

Murayama, R.; Kobayashi, M.; Jen, C. Study of Material Evaluation Probe Using a Longitudinal Wave and a Transverse Wave. *Journal of Sensor Technology* **2013,** *3*, 25–29. DOI: 10.4236/jst.2013.32005.

Nasvi, M. C. M.; Ranjith, P. G.; Sanjayan, J. Effect of different mix compositions on apparent carbon dioxide (CO_2) permeability of geopolymer: Suitability as well cement for CO_2 sequestration wells. *Applied Energy* **2014,** *114*, 939–948.

Nelson, E. B., Guillot, D., Ed. *Well Cementing*; Schlumberger Educational Services: Sugar Land, TX, 2006.

Newell, D. L.; Carey, J. W. Experimental Evaluation of Wellbore Integrity Along the Cement Rock Boundary. *Environ. Sci. Technol.* **2013,** *47*, 276–282.

Pacala, S.; Socolow, R. Stabilization Wedges: Solving the Climate Problem for the Next 50 Years with Current Technologies. *Science* **2004,** *305*, 968–972.

Pruess, K.; Müller, N. Formation dry-out from CO_2 injection into saline aquifers: 1. Effect of solids precipitation and their mitigation. *Water Resource. Res.* **2009,** *45*, W03402.

Rae, P.; Lullo, G. D. *Lightweight cement formulations for deep water cementing: Fact and fiction*; 2004; SPE 91002.

Randhol, P.; Valencia, K.; Taghipour, A.; Akervoll, I.; Carlsen, I. M. *Ensuring well integrity in connection with CO_2 injection*; SINTEF Petroleum Research; Report no. 31.6920.00/02/07; 2007.

Rasband, W. S. ImageJ; U. S. National Institutes of Health, Bethesda, Maryland, USA, 1997–2016. http://imagej.nih.gov/ij/

Scherer, G. W.; Kutchko, B.; Thaulow, N.; Duguid, A.; Mook, B. Characterization of cement from a well at Teapot Dome Oil Field: Implications for geological sequestration. *Int. J. Greenhouse Gas Control* **2011,** *5*, 115–124.

Sengers, J. V. Supercritical Fluids; Kiran, E., Levelt Sengers, J. M. H., Eds.; Kluwer, Dordrecht, 1994; 231–271.

Sommer, C.; Strähle, C.; Köthe, U.; Hamprech, F. A. ilastik: Interactive Learning and Segmentation Toolkit. Proceedings, Eighth IEEE International Symposium on Biomedical Imaging (ISBI), 2011; 230–233.

Spaulding, R. A Quantitative Assessment of Atmospherically Generated Foam Cements: Insights, Impacts, and Implications of Wellbore Integrity and Stability. Master's Thesis, University of Pittsburgh, 2015.

Spaulding, R.; Haljasmaa, I.; Fazio, J.; Gieger, C.; Kutchko, B. An Assessment of the Dynamic Moduli of Atmospherically Generated Foam Cements; 2015; OTC-25776-MS.

Spielman, P.; Hernández, R.; Nguyen, H. Reverse Circulation of Foamed Cement in Geothermal Wells. Geothermal Resources Council Annual Meeting; San Diego, CA, 2006.

Sulaiman, S. H. Water permeability and carbonation on foamed concrete. Master Thesis, University Tun Hussein Onn Malaysia, 2011.

Thaulow, N.; Lee, R. J.; Sahu, S. Effect of calcium hydroxide on the form, extent, and significance of carbonation. Calcium hydroxide in concrete; Skalny, J., Gebauer, J., Odler, I., Eds.; American Ceramic Society: Westerville, OH, 2001; 191–201.

Thayer, R. D.; Ford, D. G.; Holekamp, S.; Pferdehirt, D. J. *Real-time quality control of foamed cement jobs: A case study;* 1993; SPE 26575.

Thomas, D. Carbon Dioxide Capture for Storage in Deep Geologic Formations – Results from the CO_2 Capture Project Geologic Storage of Carbon Dioxide with Monitoring and Verification. *Technology* **2005,** *2*, 1131.

Vidas, H.; Hugman, B.; Chikkatur, A.; Venkatesh, B. *Analysis of the Costs and Benefits of CO_2 Sequestration on the U.S. Outer Continental Shelf*; U.S. Dept. of the Interior, Bureau of Ocean Energy Management: Herndon, VA, 2012; OCS Study BOEM 2012-100.

White, C.M. An Initial Set of Working Hypotheses Concerning Some Chemical and Physical Events When CO_2 Is Injected into a Coalbed; *Fuel Chem. Division Preprints* **2003,** *48*, 114–116.

White, J.; Moore, S.; Miller, M.; Faul, R. *Foaming cement as a deterrent to compaction damage in deepwater production*; 2000; IADC/SPE 59136.

APPENDIX

Table A1: Complete physical and mechanical properties of all cement samples of unreacted cement samples. Sample identification is annotated by CO_2 foamed cement; foam quality; duration. Samples that broke and measurements for Young's modulus and Poisson's ratio are highlighted in light blue.

Sample	Length (mm)	Diameter (mm)	Mass (g)	Porosity (%)	Bulk Density (g/cc)	Grain Density (g/cc)	Pore Vol (cc)	Permeability (mD)	Young's Modulus (GPa)	Poisson's ratio	1st Lame (λ) (GPa)	Bulk Modulus (GPa)	Shear Modulus (μ) (GPa)
CO_2-F-N-0 (1)	45.1	25.3	40.3	22.5	1.77	2.29	5.11	0.00271	20.0	0.208	5.9	11.4	8.28
CO_2-F-N-0 (2)	44.3	25.3	39.1	23.4	1.75	2.29	5.20	0.00478	19.6	0.201	5.48	10.9	8.16
NEAT Averages				**23.0**	**1.76**	**2.29**		0.00374	19.8	0.204	**5.69**	**11.2**	**8.22**
CO_2-F-10-0 (1)	44.3	25.2	29.2	43.4	1.33	2.35	9.55	0.0199	9.56	0.188	2.43	5.11	4.02
CO_2-F-10-0-(2)	44.5	25.0	30.4	40.8	1.39	2.35	8.89	0.00919	10.8	0.193	2.85	5.86	4.52
10% Averages				**42.1**	**1.36**	**2.35**		0.0146	10.2	0.191	**2.64**	**5.49**	**4.27**
CO_2-F-20-0 (1)	44.0	25.2	27.1	46.3	1.24	2.3	10.2	0.0143	8.82	0.196	2.37	4.83	3.69
CO_2-F-20-0 (2)	44.9	25.5	26.8	49.0	1.17	2.29	11.2	0.0408	7.56	0.185	1.87	4	3.19
20% Averages				**47.7**	**1.2**	**2.3**		0.0276	8.19	0.19	**2.12**	**4.42**	**3.44**
CO_2-F-30-0 (1)	44.2	25.2	25.1	50.4	1.14	2.29	11.1	0.0252	7.52	0.202	2.12	4.21	3.13
CO_2-F-30-0 (2)	44.5	25.0	24.5	51.2	1.12	2.29	11.2	0.0623	6.97	0.188	1.78	3.73	2.93
30% Averages				**50.8**	**1.13**	**2.29**		0.0438	7.25	0.195	**1.95**	**3.97**	**3.03**
CO_2-F-N-7	75.8	25.3	68.4	22.1	1.79	2.3	8.43	0.00579	19.9	0.212	6.08	11.6	8.22
CO_2-F-10-7	77.3	24.9	55.3	37.6	1.47	2.36	14.1	0.0102	12.4	0.208	3.65	7.08	5.14

Table A2: Complete physical and mechanical properties of the cement samples exposed to SC-CO_2

Sample	Length (mm)	Diameter (mm)	Mass (g)	Porosity (%)	Bulk Density (g/cc)	Grain Density (g/cc)	Pore Vol (cc)	Permeability (mD)	Young's Modulus (GPa)	Poisson's ratio	1st Lame (λ) (GPa)	Bulk Modulus (GPa)	Shear Modulus (μ) (GPa)
CO_2-F-20-7	75.0	25	47	45.0	1.28	2.32	16.6	0.0221	No data				
CO_2-F-30-7	76.0	25.1	44	51.5	1.67	2.4	19.4	0.0646	10.8	0.183	2.65	5.71	4.58
CO_2-F-N-14	55.6	25.1	49.3	21.0	1.79	2.26	5.77	0.00313	20.8	0.217	6.56	12.2	8.54
CO_2-F-10-14	75.0	25.3	53.6	39.7	1.42	2.35	15	0.00893	12.0	0.209	3.56	6.86	4.94
CO_2-F-20-14	76.0	25.2	46.9	47.8	1.24	2.38	18.1	0.0195	9.06	0.193	2.39	4.92	3.8
CO_2-F-30-14	75.0	25.3	44.6	50.6	1.18	2.4	19.1	0.0593	7.92	0.19	2.05	4.27	3.33
CO_2-F-N-28	74.9	25.3	68.4	21.3	1.82	2.31	8.00	0.0037	No data				
CO_2-F-10-28	73.7	25.1	55.4	35.4	1.52	2.35	12.9	0.0085	13.5	0.209	4.00	7.71	5.57
CO_2-F-20-28	74.0	24.9	46.7	46.2	1.29	2.4	16.7	0.0284	9.84	0.207	2.89	5.6	4.08
CO_2-F-30-28	73.0	25.1	43.1	50.5	1.2	2.41	18.2	0.0911	7.86	0.165	1.66	3.91	3.37
CO_2-F-N-56	73.7	25.4	67.4	19.5	1.81	2.25	7.28	0.0019	20.5	0.221	6.66	12.3	8.39
CO_2-F-10-56	54.9	25.0	40.8	30.8	1.51	2.18	8.32	0.00419	No data				
CO_2-F-20-56	66.3	25.5	44.3	43.2	1.31	2.31	14.6	0.0289	9.84	0.205	2.84	5.56	4.08
CO_2-F-30-56	70.7	25.0	43.3	47.0	1.25	2.35	16.3	0.0415	8.57	0.172	1.92	4.36	3.66

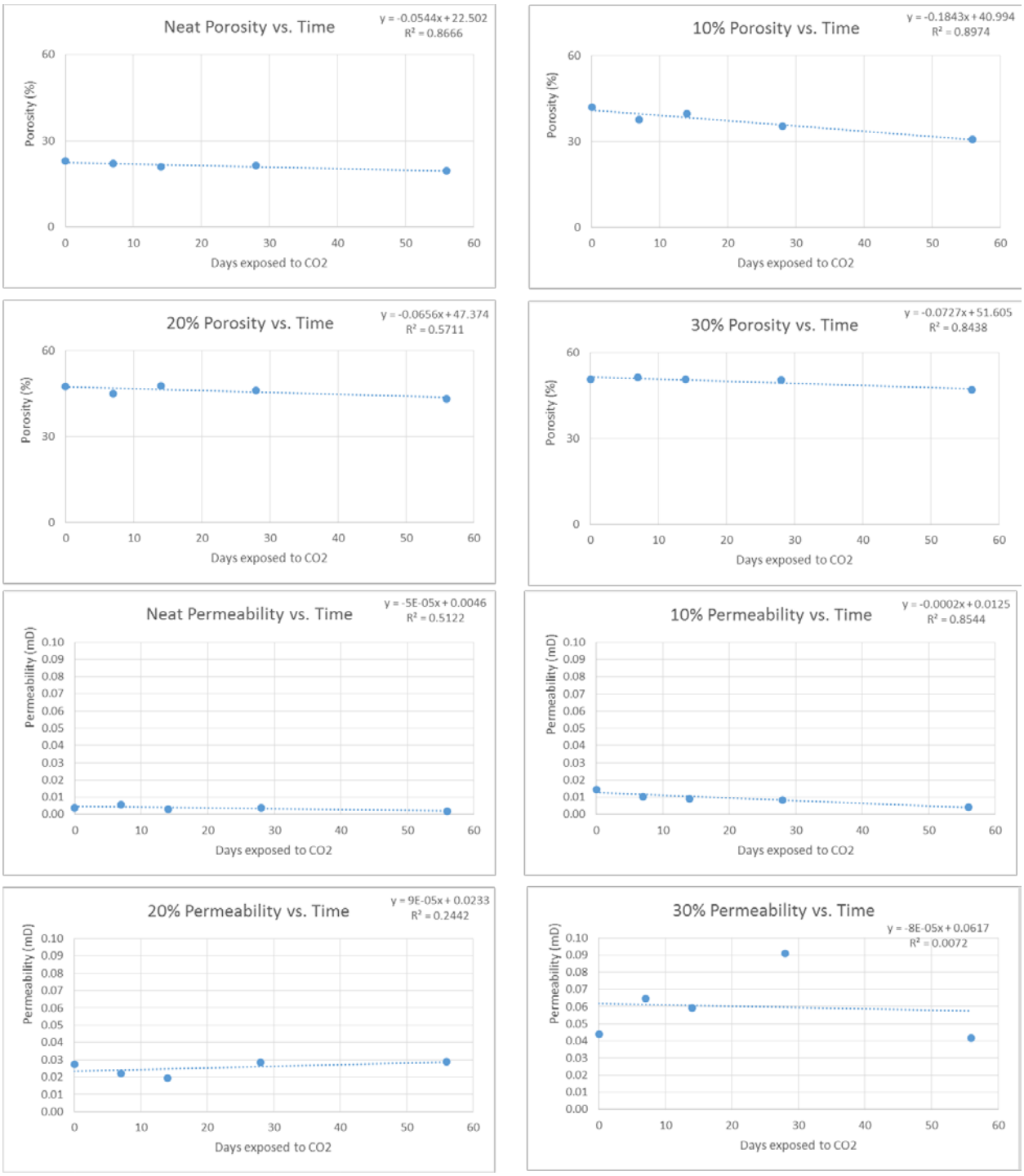

Figure A1: Correlation of A) porosity to time; B) permeability to time of reacted cement sample.

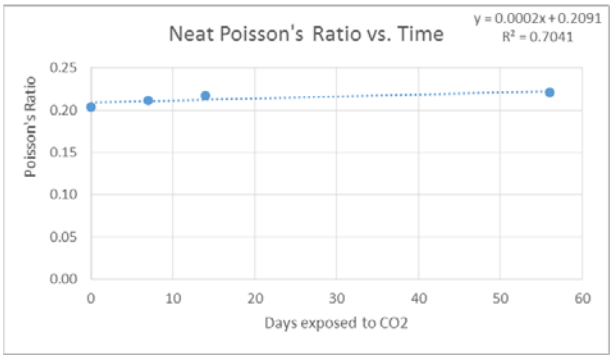

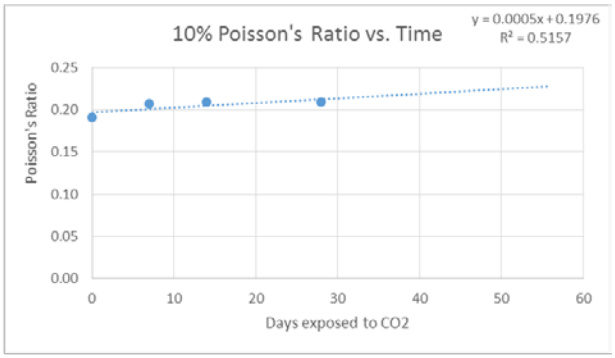

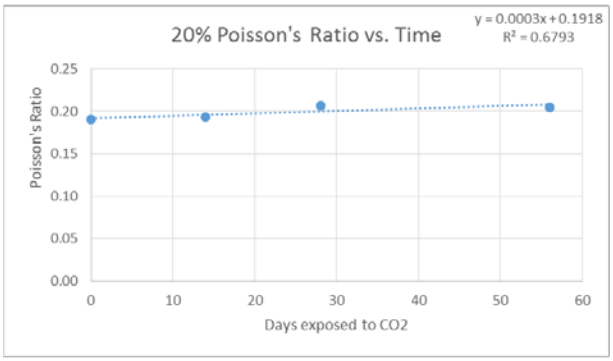

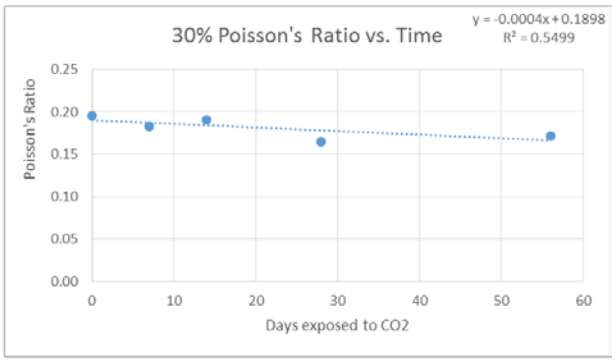

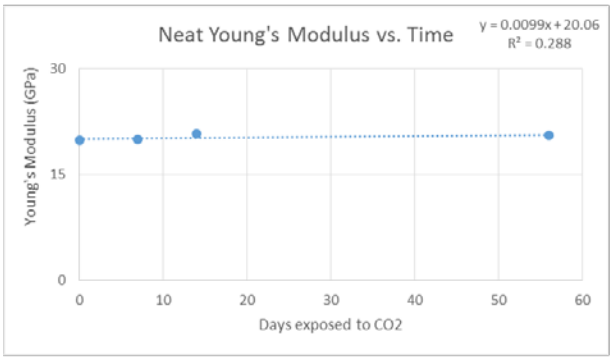

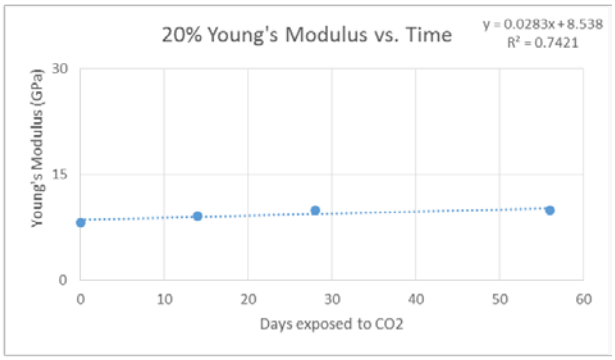

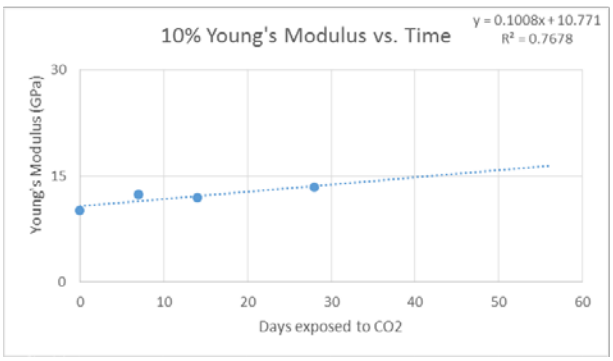

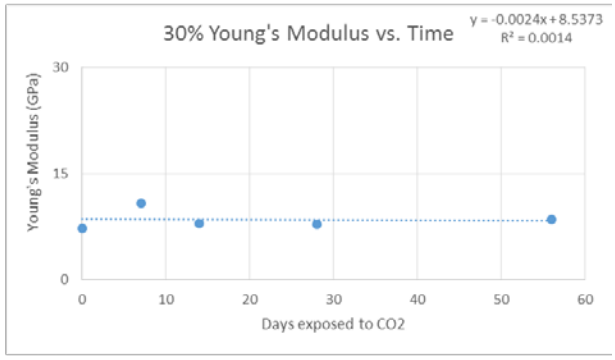

Table A2: Correlation of A) Poisson's ratio to time; B) Young's Modulus to time of reacted samples.

Sean Plasynski
Executive Director
Technology Development & Integration Center
National Energy Technology Laboratory
U.S. Department of Energy

Cynthia Powell
Executive Director
Research & Innovation Center
National Energy Technology Laboratory
U.S. Department of Energy

John Wimer
Associate Director
Strategic Planning
Science & Technology Strategic Plans & Programs
National Energy Technology Laboratory
U.S. Department of Energy

Traci Rodosta
Strategic Planning
Science & Technology Strategic Plans & Programs
National Energy Technology Laboratory
U.S. Department of Energy

Mark Ackiewicz
Director
Division of Carbon Capture and Storage
Office of Fossil Energy
U.S. Department of Energy